International Journal of Computational Methods in Engineering Science and Mechanics, 6:41–58, 2005

ISSN: 15502287 print / 15502295 online
DOI: 10.1080/15502280590888649

Taylor & Francis
healthsciences

A Meshless Method for Computational Stochastic Mechanics

S. Rahman and H. Xu
Department of Mechanical Engineering, The University of Iowa, Iowa City, IA, USA

This paper presents a stochastic meshless method for probabilistic analysis of linear-elastic structures with spatially varying random material properties. Using Karhunen-Loève (K-L) expansion, the homogeneous random field representing material properties was discretized by a set of orthonormal eigenfunctions and uncorrelated random variables. Two numerical methods were developed for solving the integral eigenvalue problem associated with K-L expansion. In the first method, the eigenfunctions were approximated as linear sums of wavelets and the integral eigenvalue problem was converted to a finite-dimensional matrix eigenvalue problem that can be easily solved. In the second method, a Galerkin-based approach in conjunction with meshless discretization was developed in which the integral eigenvalue problem was also converted to a matrix eigenvalue problem. The second method is more general than the first, and can solve problems involving a multi-dimensional random field with arbitrary covariance functions. In conjunction with meshless discretization, the classical Neumann expansion method was applied to predict second-moment characteristics of the structural response. Several numerical examples are presented to examine the accuracy and convergence of the stochastic meshless method. A good agreement is obtained between the results of the proposed method and the Monte Carlo simulation. Since mesh generation of complex structures can be far more time-consuming and costly than the solution of a discrete set of equations, the meshless method provides an attractive alternative to the finite element method for solving stochastic-mechanics problems.

Keywords Element-Free Galerkin Method, Karhunen-Loève Expansion, Meshless Method, Neumann Expansion, Random Field, Stochastic Finite Element Method, Wavelets

Received 5 November 2002; accepted 10 May 2003.

The authors would like to acknowledge the financial support of the U.S. National Science Foundation (Grant No. CMS-9900196). Dr. Ken Chong was the Program Director.

Address correspondence to S. Rahman, Department of Mechanical Engineering, The University of Iowa, Iowa City, IA 52242, USA. E-mail: rahman@engineering.uiowa.edu

1. INTRODUCTION

In recent years, much attention has been focused on collocation [1, 2] or Galerkin-based [3–8] meshfree methods to solve computational mechanics problems without using a structured grid. Among these methods, the element-free Galerkin method (EFGM) [4] is particularly appealing, due to its simplicity and its use of a formulation that corresponds to the well-established finite element method (FEM). Similar to other meshless methods, EFGM employs moving least-squares approximation [9] that permits the resultant shape functions to be constructed entirely in terms of arbitrarily placed nodes. Since no element connectivity data are needed, burdensome meshing or remeshing required by FEM is avoided. This issue is particularly important for crack propagation in solids for which FEM may become ineffective in addressing substantial remeshing [10, 11]. Hence, EFGM and other meshless methods provide an attractive alternative to FEM in solving computational-mechanics problems.

However, most developments in meshless methods have focused on deterministic problems. Research in probabilistic modeling using EFGM or other meshless methods has not been widespread and is only now gaining attention [12, 13]. For example, using perturbation expansions of response, Rahman and Rao [12] recently developed a stochastic meshless method to predict the second-moment characteristics of response for one- and two-dimensional structures. A good agreement was obtained between the results of the perturbation method and the Monte Carlo simulation when random fluctuations were small. Later, Rahman and Rao [13] incorporated the first-order reliability method in conjunction with meshless equations to predict accurate probabilistic characteristics of response and reliability. However, both of these methods involved spatial discretization of the structural domain to achieve parametric representation of the random field. This requires a large number of random variables for multi-dimensional domain discretization, and consequently, the computational effort for probabilistic meshless analysis can become very large. An alternative approach involves spectral representation of random field, such as the Karhunen-Loève expansion, which, in general, permits decomposition of random field into

fewer random variables, although their actual number depends on the covariance properties of random field. The Karhunen-Loève representation conveniently sidesteps spatial discretization of the domain, but an integral eigenvalue problem must be solved. Unfortunately, the solution of the eigenvalue problem is not an easy task. Closed-form solutions are only available when the covariance kernel has simpler functional forms. For general covariance function and arbitrary domain, numerical methods must be developed to solve the eigenvalue problem, which is a subject of the current paper. Furthermore, no stochastic methods have been developed yet using spectral properties of random field and meshless discretization. Indeed, meshless-based spectral methods for probabilistic analysis present a rich and relatively unexplored area for future research in computational stochastic mechanics.

This paper presents a stochastic meshfree method for solving solid-mechanics problems in linear elasticity that involves random material properties. Using Karhunen-Loève expansion, the random field representing material properties was modeled by a linear sum of orthonormal eigenfunctions with uncorrelated random coefficients. Two numerical methods were developed for solving the integral eigenvalue problem associated with K-L expansion. In the first method, the eigenfunctions were approximated as linear sums of wavelets and the integral eigenvalue problem was converted to a finite-dimensional matrix eigenvalue problem that can be easily solved. In the second method, a Galerkin-based approach in conjunction with meshless discretization was developed in which the integral eigenvalue problem was also converted to a matrix eigenvalue problem. In conjunction with meshless equations, the Neumann expansion method was applied to predict second-moment characteristics of structural response. Several numerical examples are presented to illustrate the proposed method.

2. THE ELEMENT-FREE GALERKIN METHOD

2.1. Moving Least Squares and Meshless Shape Function

Consider a function $u(\mathbf{x})$ over a domain $\Omega \subseteq \Re^K$, where $K = 1$, 2, or 3. Let $\Omega_{\boldsymbol{x}} \subseteq \Omega$ denote a sub-domain describing the neighborhood of a point $\mathbf{x} \in \Re^K$ located in Ω. According to the moving least-squares (MLS) [9] method, the approximation $u^h(\mathbf{x})$ of $u(\mathbf{x})$ is

$$u^h(\mathbf{x}) = \sum_{i=1}^{m} p_i(\mathbf{x}) a_i(\mathbf{x}) \; = \mathbf{p}^T(\mathbf{x})\mathbf{a}(\mathbf{x}), \qquad [1]$$

where $\mathbf{p}^T(\mathbf{x}) = \{p_1(\mathbf{x}), p_2(\mathbf{x}), \ldots, p_m(\mathbf{x})\}$ is a vector of complete basis functions of order m and $\mathbf{a}(\mathbf{x}) = \{a_1(\mathbf{x}), a_2(\mathbf{x}), \ldots, a_m(\mathbf{x})\}$ is a vector of unknown parameters that depend on x. For example, in two dimensions ($K = 2$) with x_1- and x_2-coordinates,

$$\mathbf{p}^T(\mathbf{x}) = \{1, x_1, x_2\}, m = 3 \qquad [2]$$

and

$$\mathbf{p}^T(\mathbf{x}) = \left\{1, x_1, x_2, x_1^2, x_1x_2, x_2^2\right\}, m = 6 \qquad [3]$$

representing the linear and quadratic basis functions, respectively, are commonly used in solid mechanics.

In Eq. (1), the coefficient vector $\mathbf{a}(\mathbf{x})$ is determined by minimizing a weighted discrete $\mathcal{L}_2$ norm, defined as

$$\begin{aligned} J(\mathbf{x}) &= \sum_{I=1}^{n} w_I(\mathbf{x})[\mathbf{p}^T(\mathbf{x}_I)\mathbf{a}(\mathbf{x}) - d_I]^2 \\ &= [\mathbf{P}\mathbf{a}(\mathbf{x}) - \mathbf{d}]^T\mathbf{W}[\mathbf{P}\mathbf{a}(\mathbf{x}) - \mathbf{d}], \end{aligned} \qquad [4]$$

where $\mathbf{x}_I$ denotes the coordinates of node I, $\mathbf{d}^T = \{d_1, d_2, \ldots, d_n\}$ with d_I representing the nodal parameter for node I, $\mathbf{W} = \text{diag}\,[w_1(\mathbf{x}), w_2(\mathbf{x}), \ldots, w_n(\mathbf{x})]$ with $w_I(\mathbf{x})$ the weight function associated with node I such that $w_I(\mathbf{x}) > 0$ for all $\mathbf{x}$ in the support $\Omega_{\mathbf{x}}$ of $w_I(\mathbf{x})$ and *zero* otherwise, n is the number of nodes in $\Omega_{\mathbf{x}}$ for which $w_I(\mathbf{x}) > 0$, and

$$\mathbf{P} = \begin{bmatrix} \mathbf{p}^T(\mathbf{x}_1) \\ \mathbf{p}^T(\mathbf{x}_2) \\ \vdots \\ \mathbf{p}^T(\mathbf{x}_n) \end{bmatrix} \in \mathcal{L}(\Re^n \times \Re^m). \qquad [5]$$

A number of weight functions are available in the current literature [3–8, 10, 11]. In this study, a weight function proposed by Rao and Rahman [11] was used, which is

$$w_I(\mathbf{x}) = \begin{cases} \dfrac{\left(1 + \beta^2 \frac{z_I^2}{z_{mI}^2}\right)^{-\left(\frac{1+\beta}{2}\right)} - (1+\beta^2)^{-\left(\frac{1+\beta}{2}\right)}}{1 - (1+\beta^2)^{-\left(\frac{1+\beta}{2}\right)}}, & z_I \le z_{mI} \\ 0, & z_I > z_{mI} \end{cases} \qquad [6]$$

where β is a parameter controlling the shape of the weight function, $z_I = ||\mathbf{x} - \mathbf{x}_I||$ is the distance from a sample point $\mathbf{x}$ to a node $\mathbf{x}_I$, and z_{mI} is the domain of influence of node I. The stationarity of $J(\mathbf{x})$ with respect to $\mathbf{a}(\mathbf{x})$ yields

$$\mathbf{A}(\mathbf{x})\mathbf{a}(\mathbf{x}) = \mathbf{C}(\mathbf{x})\mathbf{d}, \qquad [7]$$

where

$$\mathbf{A}(\mathbf{x}) = \sum_{I=1}^{n} w_I(\mathbf{x})\mathbf{p}(\mathbf{x}_I)\mathbf{p}^T(\mathbf{x}_I) = \mathbf{P}^T\mathbf{W}\mathbf{P} \qquad [8]$$

and

$$\mathbf{C}(\mathbf{x}) = [w_1(\mathbf{x})\mathbf{p}(\mathbf{x}_1), \ldots, w_n(\mathbf{x})\mathbf{p}(\mathbf{x}_n)] = \mathbf{P}^T\mathbf{W}. \qquad [9]$$

Solving for $\mathbf{a}(\mathbf{x})$ in Eq. (7) and then substituting into Eq. (1) yields

$$u^h(\mathbf{x}) = \sum_{I=1}^{n} \mathbf{\Phi}_I(\mathbf{x}) d_I = \mathbf{\Phi}^T(\mathbf{x})\mathbf{d}, \qquad [10]$$

where

$$\mathbf{\Phi}^T(\mathbf{x}) = \{\Phi_1(\mathbf{x}), \Phi_2(\mathbf{x}), \ldots \Phi_n(\mathbf{x})\} = \mathbf{p}^T(\mathbf{x})\mathbf{A}^{-1}(\mathbf{x})\mathbf{C}(\mathbf{x}) \quad [11]$$

is a vector with its Ith component,

$$\Phi_I(\mathbf{x}) = \sum_{j=1}^{m} p_j(\mathbf{x})[\mathbf{A}^{-1}(\mathbf{x})\mathbf{C}(\mathbf{x})]_{jI}, \quad [12]$$

representing the shape function of the MLS approximation corresponding to node I. The partial derivatives of $\mathbf{\Phi}_I(\mathbf{x})$ can also be obtained as

$$\Phi_{I,i}(\mathbf{x}) = \sum_{j=1}^{m} \left\{ p_{j,i}(\mathbf{A}^{-1}\mathbf{C})_{jI} + p_j\left(\mathbf{A}^{-1}_{,i}\mathbf{C} + \mathbf{A}^{-1}\mathbf{C}_{,i}\right)_{jI} \right\}, \quad [13]$$

where $\mathbf{A}^{-1}_{,i} = -\mathbf{A}^{-1}\mathbf{A}_{,i}\mathbf{A}^{-1}$ and $(\,)_{,i} = \partial(\,)/\partial x_i$.

2.2. Variational Formulation and Discretization

For small displacements in two-dimensional, isotropic, and linear-elastic solids, the equilibrium equations and boundary conditions are

$$\nabla \cdot \boldsymbol{\sigma} + \mathbf{b} = 0 \text{ in } \Omega \quad [14]$$

and

$$\begin{array}{ll} \boldsymbol{\sigma} \cdot \mathbf{n} = \bar{\mathbf{t}} & \text{on } \Gamma_t \text{ (natural boundary conditions)} \\ \mathbf{u} = \bar{\mathbf{u}} & \text{on } \Gamma_u \text{ (essential boundary conditions)'} \end{array} \quad [15]$$

respectively, where $\boldsymbol{\sigma} = \mathbf{D}\boldsymbol{\varepsilon}$ is the stress vector, $\mathbf{D}$ is the material property matrix, $\boldsymbol{\varepsilon} = \nabla_s\mathbf{u}$ is the strain vector, $\mathbf{u}$ is the displacement vector, $\mathbf{b}$ is the body force vector, $\bar{\mathbf{t}}$ and $\bar{\mathbf{u}}$ are the vectors of prescribed surface tractions and displacements, respectively, $\mathbf{n}$ is a unit normal to the domain, Ω, Γ_t and Γ_u are the portions of boundary Γ where tractions and displacements are respectively prescribed, $\nabla^T = \{\partial/\partial x_1, \partial/\partial x_2\}$ is the vector of gradient operators, and $\nabla_s\mathbf{u}$ is the symmetric part of $\nabla\mathbf{u}$. The variational or weak form of Eqs. (14) and (15) is

$$\int_\Omega \boldsymbol{\sigma}^T \delta\boldsymbol{\varepsilon} d\Omega - \int_\Omega \mathbf{b}^T \delta\mathbf{u} d\Omega - \int_{\Gamma_t} \bar{\mathbf{t}}^T \delta\mathbf{u} d\Gamma + \delta W_u = 0, \quad [16]$$

where δ denotes the variation operator and δW_u represents a term that enforces essential boundary conditions. The explicit form of this term depends on the method by which the essential boundary conditions are imposed [4, 10–12]. In this study, W_u is defined as

$$W_u = \sum_{x_J \in \Gamma_u} \mathbf{f}^T(\mathbf{x}_J)[\mathbf{u}(\mathbf{x}_J) - \bar{\mathbf{u}}(\mathbf{x}_J)], \quad [17]$$

where $\mathbf{f}^T(\mathbf{x}_J)$ is the vector of reaction forces at the constrained node $J \in \Gamma_u$. Hence,

$$\delta W_u = \sum_{x_J \in \Gamma_u} \delta\mathbf{f}^T(\mathbf{x}_J)[\mathbf{u}(\mathbf{x}_J) - \bar{\mathbf{u}}(\mathbf{x}_J)] + \mathbf{f}^T(\mathbf{x}_J)\delta\mathbf{u}(\mathbf{x}_J). \quad [18]$$

Consider a single boundary constraint $\bar{u}_i(\mathbf{x}_J) = g_i(\mathbf{x}_J)$ applied at node J in the direction of the x_i coordinate. The variational form given by Eqs. (16) and (18) can then be expressed by

$$\int_\Omega \boldsymbol{\sigma}^T \delta\boldsymbol{\varepsilon} d\Omega + f_i(\mathbf{x}_J)\delta u_i(\mathbf{x}_J) = \int_\Omega \mathbf{b}^T \delta\mathbf{u} d\Omega + \int_{\Gamma_t} \bar{\mathbf{t}}^T \delta\mathbf{u} d\Gamma \quad [19]$$

$$\delta f_i(\mathbf{x}_J)[u_i(\mathbf{x}_J) - g_i(\mathbf{x}_J)] = 0, \quad [20]$$

where $f_i(\mathbf{x}_J)$ and $u_i(\mathbf{x}_J)$ are the ith component of $\mathbf{f}(\mathbf{x}_J)$ and $\mathbf{u}(\mathbf{x}_J)$, respectively. From Eq. (10), the MLS approximation of $u_i(\mathbf{x}_J)$ is

$$u_i^h(\mathbf{x}_J) = \sum_{I=1}^{N} \mathbf{\Phi}_I(\mathbf{x}_J) d_I^i = \mathbf{\Phi}_J^{iT}\mathbf{d}, \quad [21]$$

where

$$\mathbf{\Phi}_J^{iT} = \begin{cases} \{\Phi_1(\mathbf{x}_J), 0, \Phi_2(\mathbf{x}_J), 0, \ldots, \Phi_N(\mathbf{x}_J), 0\}, & \text{when } i = 1 \\ \{0, \Phi_1(\mathbf{x}_J), 0, \Phi_2(\mathbf{x}_J), \ldots, 0, \Phi_N(\mathbf{x}_J)\}, & \text{when } i = 2 \end{cases} \quad [22]$$

$$\mathbf{d} = \begin{Bmatrix} d_1^1 \\ d_1^2 \\ d_2^1 \\ d_2^2 \\ \vdots \\ d_N^1 \\ d_N^2 \end{Bmatrix} \quad [23]$$

is the vector of nodal parameters or generalized displacements, and N is the total number of nodal points in Ω. Applying Eqs. (21–23) to the discretization of Eqs. (19) and (20) yields [4, 10, 11]

$$\begin{bmatrix} \mathbf{k} & \mathbf{\Phi}_J^i \\ \mathbf{\Phi}_J^{iT} & 0 \end{bmatrix} \begin{Bmatrix} \mathbf{d} \\ f_i(\mathbf{x}_J) \end{Bmatrix} = \begin{Bmatrix} \mathbf{f}^{ext} \\ g_i(\mathbf{x}_J) \end{Bmatrix}, \quad [24]$$

where

$$\mathbf{k} = \begin{bmatrix} \mathbf{k}_{11} & \mathbf{k}_{12} & \cdots & \mathbf{k}_{1N} \\ \mathbf{k}_{21} & \mathbf{k}_{22} & \cdots & \mathbf{k}_{2N} \\ \vdots & \vdots & \vdots & \vdots \\ \mathbf{k}_{N1} & \mathbf{k}_{N2} & \cdots & \mathbf{k}_{NN} \end{bmatrix} \in \mathcal{L}\left(\Re^{2N} \times \Re^{2N}\right) \quad [25]$$

is the stiffness matrix with

$$\mathbf{k}_{IJ} = \int_{\Omega} \mathbf{B}_I^T \mathbf{D} \mathbf{B}_J d\Omega \in \mathcal{L}(\Re^2 \times \Re^2), \tag{26}$$

representing the contributions of the Jth node at node I,

$$\mathbf{f}^{ext} = \begin{Bmatrix} \mathbf{f}_1^{ext} \\ \mathbf{f}_2^{ext} \\ \vdots \\ \mathbf{f}_N^{ext} \end{Bmatrix} \in \Re^{2N} \tag{27}$$

is the force vector with

$$\mathbf{f}_I^{ext} = \int_{\Omega} \mathbf{\Phi}_I \mathbf{b}^T d\Omega + \int_{\Gamma_t} \mathbf{\Phi}_I \bar{\mathbf{t}}^T d\Gamma \in \Re^2, \tag{28}$$

$$\mathbf{B}_I = \begin{bmatrix} \mathbf{\Phi}_{I,1} & 0 \\ 0 & \mathbf{\Phi}_{I,2} \\ \mathbf{\Phi}_{I,2} & \mathbf{\Phi}_{I,1} \end{bmatrix}, \tag{29}$$

and

$$\mathbf{D} = \begin{cases} \frac{E}{1-\nu^2} \begin{bmatrix} 1 & \nu & 0 \\ \nu & 1 & 0 \\ 0 & 0 & \frac{1-\nu}{2} \end{bmatrix}, & \text{for plane stress} \\ \frac{E}{(1+\nu)(1-2\nu)} \begin{bmatrix} 1-\nu & \nu & 0 \\ \nu & 1-\nu & 0 \\ 0 & 0 & \frac{1-2\nu}{2} \end{bmatrix}, & \text{for plane strain} \end{cases} \tag{30}$$

is the elasticity matrix with E and ν representing the elastic modulus and Poisson's ratio, respectively. To perform numerical integration in Eqs. (26) and (28), a background mesh is required, which can be independent of the arrangement of the meshless nodes. However, in this study, the nodes of the background mesh coincide with the meshless nodes. Standard Gaussian quadratures were used to evaluate the integrals for assembling the stiffness matrix and the force vector. In general, a 4×4 quadrature rule is adequate, except in the cells surrounding a high stress gradient (e.g., near a crack tip) where a 8×8 quadrature rule is suggested.

2.3. Essential Boundary Conditions

In solving for $\mathbf{d}$, essential boundary conditions must be enforced. The lack of Kronecker delta properties in the meshless shape functions presents some difficulty in imposing the essential boundary conditions in EFGM. Nevertheless, several methods are currently available for enforcing essential boundary conditions. A transformation method [11, 14] was used for the stochastic-mechanics application in this work.

Consider the transformation

$$\hat{\mathbf{d}} = \mathbf{\Lambda} \mathbf{d}, \tag{31}$$

where

$$\hat{\mathbf{d}} = \begin{Bmatrix} u_1^h(\mathbf{x}_1) \\ u_2^h(\mathbf{x}_1) \\ u_1^h(\mathbf{x}_2) \\ u_2^h(\mathbf{x}_2) \\ \vdots \\ u_1^h(\mathbf{x}_N) \\ u_2^h(\mathbf{x}_N) \end{Bmatrix} \in \Re^{2N} \tag{32}$$

is the nodal displacement vector, and

$$\Lambda = \begin{bmatrix} \mathbf{\Phi}_1^{1T} \\ \mathbf{\Phi}_1^{2T} \\ \mathbf{\Phi}_2^{1T} \\ \mathbf{\Phi}_2^{2T} \\ \vdots \\ \mathbf{\Phi}_N^{1T} \\ \mathbf{\Phi}_N^{2T} \end{bmatrix} \in \mathcal{L}\left(\Re^{2N} \times \Re^{2N}\right) \tag{33}$$

is the transformation matrix. Multiplying the first set of matrix equations in Eq. (24) by $\mathbf{\Lambda}^{-T}$, one obtains

$$\begin{bmatrix} \mathbf{\Lambda}^{-T}\mathbf{k} & \mathbf{I}_J^i \\ \mathbf{\Phi}_J^{iT} & 0 \end{bmatrix} \begin{Bmatrix} \mathbf{d} \\ f_i(\mathbf{x}_J) \end{Bmatrix} = \begin{Bmatrix} \mathbf{\Lambda}^{-T}\mathbf{f}^{ext} \\ g_i(\mathbf{x}_J) \end{Bmatrix} \tag{34}$$

where

$$\mathbf{I}_J^i = \mathbf{\Lambda}^{-T} \mathbf{\Phi}_J^i = \begin{Bmatrix} 0 \\ \vdots \\ 0 \\ 1 \\ 0 \\ \vdots \\ 0 \end{Bmatrix} \leftarrow [2(J-1)+i]\text{th row.} \tag{35}$$

Let

$$\hat{\mathbf{k}} = \begin{bmatrix} \hat{\mathbf{k}}_1^T \\ \vdots \\ \hat{\mathbf{k}}_{2N}^T \end{bmatrix} = \mathbf{\Lambda}^{-T}\mathbf{k} \tag{36}$$

and

$$\hat{\mathbf{f}}^{ext} = \mathbf{\Lambda}^{-T}\mathbf{f}^{ext}, \tag{37}$$

where $\hat{\mathbf{k}}_i^T = \{\hat{k}_{i1}, \hat{k}_{i2}, \ldots \hat{k}_{i(2N)}\}$, $i = 1, 2, \ldots, 2N$. Eq. (34) can be re-written as

$$\begin{bmatrix} \hat{\mathbf{k}}_1^T & 0 \\ \vdots & \vdots \\ \hat{\mathbf{k}}_{M-1}^T & 0 \\ \hat{\mathbf{k}}_M^T & 1 \\ \hat{\mathbf{k}}_{M+1}^T & 0 \\ \vdots & \vdots \\ \hat{\mathbf{k}}_{2N}^T & 0 \\ \boldsymbol{\Phi}_J^{iT} & 0 \end{bmatrix} \begin{Bmatrix} \mathbf{d} \\ f_i(\mathbf{x}_J) \end{Bmatrix} = \begin{Bmatrix} \hat{f}_1^{ext} \\ \vdots \\ \hat{f}_{M-1}^{ext} \\ \hat{f}_M^{ext} \\ \hat{f}_{M+1}^{ext} \\ \vdots \\ \hat{f}_{2N}^{ext} \\ g_i(\mathbf{x}_J) \end{Bmatrix} \begin{matrix} \\ \\ \\ \leftarrow [2(J-1)+i]\text{th row} \\ \\ \\ \leftarrow (2N+1)\text{th row} \end{matrix}, \quad [38]$$

where $M = (2J-1)+i$. Exchanging the Mth with the last row of Eq. (38) leads to

$$\begin{bmatrix} \hat{\mathbf{k}}_1^T & 0 \\ \vdots & \vdots \\ \hat{\mathbf{k}}_{M-1}^T & 0 \\ \boldsymbol{\Phi}_J^{iT} & 0 \\ \hat{\mathbf{k}}_{M+1}^T & 0 \\ \vdots & \vdots \\ \hat{\mathbf{k}}_{2N}^T & 0 \\ \hat{\mathbf{k}}_M^T & 1 \end{bmatrix} \begin{Bmatrix} \mathbf{d} \\ f_i(\mathbf{x}_J) \end{Bmatrix} = \begin{Bmatrix} \hat{f}_1^{ext} \\ \vdots \\ \hat{f}_{M-1}^{ext} \\ g_i(\mathbf{x}_J) \\ \hat{f}_{M+1}^{ext} \\ \vdots \\ \hat{f}_{2N}^{ext} \\ \hat{f}_M^{ext} \end{Bmatrix} \begin{matrix} \\ \\ \\ \leftarrow [2(J-1)+i]\,\text{th row} \\ \\ \\ \leftarrow (2N+1)\text{th row} \end{matrix}, \quad [39]$$

which can be uncoupled as

$$\mathbf{K}\mathbf{d} = \mathbf{F} \quad [40]$$

$$\hat{\mathbf{k}}_M^T \mathbf{d} + f_i(\mathbf{x}_J) = \hat{f}_M^{ext}, \quad [41]$$

where

$$\mathbf{K} = \boldsymbol{\mathcal{M}}_J^i(\hat{\mathbf{k}}) = \begin{bmatrix} \hat{\mathbf{k}}_1^T \\ \vdots \\ \hat{\mathbf{k}}_{M-1}^T \\ \boldsymbol{\Phi}_J^{iT} \\ \hat{\mathbf{k}}_{M+1}^T \\ \vdots \\ \vdots \\ \hat{\mathbf{k}}_{2N}^T \end{bmatrix} \leftarrow [2(J-1)+i]\text{th row} \quad [42]$$

and

$$\mathbf{F} = \boldsymbol{\mathcal{N}}_J^i(\hat{f}^{ext}) = \begin{bmatrix} \hat{f}_1^{ext} \\ \vdots \\ \hat{f}_{M-1}^T \\ g_i(\mathbf{x}_J) \\ \hat{f}_{M+1}^{ext} \\ \vdots \\ \vdots \\ \hat{f}_{2N}^{ext} \end{bmatrix} \leftarrow [2(J-1)+i]\text{th row} \quad [43]$$

are the modified stiffness matrix and force vectors, respectively. Using Eq. (40), the generalized displacement vector $\mathbf{d}$ can be solved efficiently without the need for any Lagrange multipliers [4, 10, 15].

In Eqs. (42) and (43), $\boldsymbol{\mathcal{M}}_J^i$ is a matrix operator that replaces the $[2(J-1)+i]$th row of $\hat{\mathbf{k}}$ by $\boldsymbol{\Phi}_J^{iT}$ and $\boldsymbol{\mathcal{N}}_J^i$ is another matrix operator that replaces the $[2(J-1)+i]$th row of $\hat{\mathbf{f}}^{ext}$ by $g_i(\mathbf{x}_J)$, due to the application of a single boundary constraint at node J. For multiple boundary constraints, similar operations can be repeated. Suppose that there are an N_c number of essential boundary conditions at nodes $J_1, J_2, \ldots, J_{N_c}$ applied in the directions, $i_1, i_2, \ldots, i_{N_c}$, respectively. Hence, the resulting modified stiffness matrix and force vector are

$$\mathbf{K} = \prod_{l=1}^{N_c} \boldsymbol{\mathcal{M}}_{J_l}^{i_l}(\hat{\mathbf{k}}) \quad [44]$$

and

$$\mathbf{F} = \prod_{l=1}^{N_c} \boldsymbol{\mathcal{N}}_{J_l}^{i_l}(\hat{\mathbf{f}}^{ext}), \quad [45]$$

respectively.

3. RANDOM FIELD AND PARAMETERIZATION

3.1. Random Field

Assume that the spatial variability of material property, such as the elastic modulus $E(\mathbf{x})$, can be modeled as a homogeneous random field, given by

$$E(\mathbf{x}) = \mu_E[1 + \alpha(\mathbf{x})], \quad [46]$$

where $\mu_E = \boldsymbol{\mathcal{E}}[E(\mathbf{x})] \neq 0$ is the constant mean of elastic modulus, $\alpha(\mathbf{x}) \in \Re$ is a zero-mean, scalar, homogeneous random field with its auto-covariance function $\Gamma_\alpha(\boldsymbol{\xi}) = \boldsymbol{\mathcal{E}}[\alpha(\mathbf{x})\alpha(\mathbf{x}+\boldsymbol{\xi})]$, $\boldsymbol{\xi}$ is the separation vector between two points, $\mathbf{x}_1 = \mathbf{x} \in \Re^K$ and $\mathbf{x}_2 = \mathbf{x} + \boldsymbol{\xi} \in \Re^K$ both located in $\Omega \subseteq \Re^K$, and $\boldsymbol{\mathcal{E}}[\cdot]$ is the expectation operator.

In stochastic finite element or meshless applications, it is necessary to discretize a continuous-parameter random field (e.g., Eq. (46)) into a vector of random variables. Various discretization methods have been developed, such as Karhunen-Loève expansion (K-L) [16], the basis random variables method [17] the midpoint method [18], the local averaging method [19], the shape function method [20], the weighted-integral method [21], the optimal linear estimation method [22] and others. Among these methods, Li and Der Kiureghian [22] found K-L expansion to be one of the most efficient methods for parameterizing a random field.

3.2. Karhunen-Loève Expansion

Let $\{\lambda_i, f_i(\mathbf{x})\}$, $i = 1, 2, \ldots, \infty$, be the eigenvalues and eigenfunctions of the continuous, bounded, symmetric, and positive-definite covariance kernel $\Gamma(\mathbf{x}_1, \mathbf{x}_2) = \Gamma_\alpha(\boldsymbol{\xi})$ of $\alpha(\mathbf{x})$. They satisfy the integral Eq. (23)

$$\int_\Omega \Gamma(\mathbf{x}_1, \mathbf{x}_2) f_i(\mathbf{x}_2) d\mathbf{x}_2 = \lambda_i f_i(\mathbf{x}_1), \quad \forall i = 1, 2, \ldots, \infty, \quad [47]$$

where $\Omega \in \Re^K$ is the domain over which the random field is defined. The eigenfunctions are orthogonal in the sense that

$$\int_\Omega f_i(\mathbf{x}) f_j(\mathbf{x}) d\mathbf{x} = \delta_{ij}, \quad \forall i, j = 1, 2, \ldots, \infty, \quad [48]$$

where δ_{ij} is the Kronecker delta. The parametric random field

$$\hat{\alpha}_M(\mathbf{x}) = \sum_{i=1}^{M} U_i \sqrt{\lambda_i} f_i(\mathbf{x}), \quad [49]$$

which represents K-L expansion, approaches $\alpha(\mathbf{x})$ in the mean square sense for $\mathbf{x} \in \Omega$ as $M \to \infty$. In Eq. (49), U_i, $i = 1, 2, \ldots, M$ are uncorrelated random variables, each of which has zero mean and unit variance. If $\alpha(\mathbf{x})$ is a Gaussian random field, $\mathbf{U} = \{U_1, U_2, \ldots, U_M\}^T \in \Re^M$ becomes an M-dimensional standard Gaussian vector.

K-L expansion given by Eq. (49) is quite useful in stochastic mechanics, because it provides a parametric representation of an arbitrary random field with bounded covariance functions. This representation does not require any spatial discretization of the domain. However, in general the solution of the associated eigenvalue problem (i.e., solving Eq. (47)) is not an easy task. Closed-form solutions are only available when the covariance kernel has simpler functional forms, such as exponential and linear functions [16]. When the covariance function is more complex, numerical methods are needed to solve the eigenvalue problem. In this study, two numerical methods based on wavelets and meshless discretization are proposed to solve the eigenvalue problem.

4. SOLUTION OF INTEGRAL EIGENVALUE PROBLEM

4.1. Wavelet Method

Wavelets constitute a family of functions constructed from dilation and translation of a single function called the mother wavelet. For $x \in \Re$, consider a family of extended Haar wavelets (EHW), defined as [24]

$$\psi_{s,t}(x) = A_s \psi(2^s x - t), \quad [50]$$

where s and t are the dilation and translational parameters, $A_s = 2^{s/2}$ is the amplitude, and

$$\psi(x) = \begin{cases} 1, & x \in [0, 1/2) \\ -1, & x \in [1/2, 1) \\ 0, & \text{otherwise} \end{cases} \quad [51]$$

is the Haar function. Let

$$\psi_0(x) = 1 \text{ and} \quad [52]$$

$$\psi_i(x) = \psi_{s,t}(x), \quad [53]$$

where $i = 2^s + t$, $s = 0, 1, \ldots$, and $t = 0, \ldots, 2^s - 1$. It can be shown that the EHW basis functions, defined by Eqs. (52) and (53), constitute a complete orthonormal set over the domain [0, 1].

For a one-dimensional random field in [0, 1], consider a Z-order wavelet expansion of the covariance function and its ith eigenfunction, given by

$$\Gamma(x_1, x_2) = \sum_{i=0}^{Z} \sum_{j=0}^{Z} H_{ij} \psi_i(x_1) \psi_j(x_2) = \boldsymbol{\Psi}^T(x_1) \mathbf{H} \boldsymbol{\Psi}(x_2) \quad [54]$$

$$f_i(x) = \sum_{j=0}^{Z} v_{ij} \psi_j(x) = \boldsymbol{\Psi}^T(x) \boldsymbol{v}_i, \quad [55]$$

where $\boldsymbol{\Psi}^T(x) = \{\psi_0(x), \psi_1(x), \ldots, \psi_z(x)\}$, $\boldsymbol{v}_i^T = \{v_{i0}, v_{i1} \cdots, v_{iz}\}$, and $\mathbf{H} = [H_{ij}]$ with $H_{ij} = \int_0^1 \int_0^1 \Gamma(x_1, x_2) \psi_i(x_1) \psi_j(x_2) dx_1 dx_2$. Using Eqs. (54) and (55), Eq. (47) simplifies to a matrix eigenvalue problem

$$\lambda_i \boldsymbol{v}_i = \mathbf{H} \boldsymbol{v}_i, \quad [56]$$

which is a finite dimensional representation of the integral eigenvalue problem in Eq. (47) for $x \in \Re$. Eq. (56) can be formulated for any covariance function of a one-dimensional random field and can be easily solved using standard methods of linear algebra. Once the eigenvector $\mathbf{v}_i$ is calculated, Eq. (55) can be used to determine the eigenfunction $f_i(x)$.

For a multi-dimensional random field ($\mathbf{x} \in \Re^K$) with a rectangular domain, if the covariance function is separable to support a multiplicative decomposition of the form

$$\Gamma(\mathbf{x}_1, \mathbf{x}_2) = \prod_{i=1}^{K} \Gamma_i(x_{1i}, x_{2i}), \quad [57]$$

where x_{1i} and x_{2i} are the ith coordinates of two points in $\Re^K$ and $\Gamma(x_{1i}, x_{2i})$ is the ith function, then similar wavelet approximation can be applied to $\Gamma(x_1, x_2)$. In that case, Eq. (47) also becomes separable and only requires solving one-dimensional eigenvalue problem similar to the one described by Eq. (56). However, wavelet-based methods may not be effective or applicable if the domain of a multi-dimensional random field is irregular (i.e., any arbitrary shape in $\Re^K$ and/or is associated with a general covariance function. Hence, more general methods are needed to solve the eigenvalue problem.

4.2. Meshless Method

For a multi-dimensional random field ($\mathbf{x} \in \Re^K$) with arbitrary domain $\Omega \subseteq \Re^K$, consider an MLS approximation of the eigenfunction $f_i(\mathbf{x})$, given by

$$f_i(\mathbf{x}) = \sum_{I=1}^{N} \hat{f}_{iI} \mathbf{\Phi}_1(\mathbf{x}), \qquad [58]$$

where $\hat{f}_{iI}$ is the Ith nodal parameter for the ith eigenfunction, $\mathbf{\Phi}_I(\mathbf{x})$ is the meshless shape function of the Ith node, and N is the total number of nodes. Using Eq. (58), Eq. (47) becomes

$$\sum_{I=1}^{N} \hat{f}_{iI} \int_{\Omega} \Gamma(\mathbf{x}_1, \mathbf{x}_2) \Phi_I(\mathbf{x}_2) d\mathbf{x}_2 = \lambda_i \sum_{I=1}^{N} \hat{f}_{iI}\, \mathbf{\Phi}_I(\mathbf{x}_1). \qquad [59]$$

Define

$$\varepsilon_N = \sum_{I=1}^{N} \hat{f}_{iI} \left(\int_{\Omega} \Gamma(\mathbf{x}_1, \mathbf{x}_2) \mathbf{\Phi}_I(\mathbf{x}_2) d\mathbf{x}_2 - \lambda_i \mathbf{\Phi}_I(\mathbf{x}_1) \right) \qquad [60]$$

as the residual error, which is associated with meshless discretization involving an N number of nodes. Following Galerkin approximation,

$$\int_{\Omega} \varepsilon_N \mathbf{\Phi}_J(\mathbf{x}_1) d\mathbf{x}_1 = 0, \quad \forall J = 1, \ldots, N, \qquad [61]$$

which, when combined with Eq. (60), can be expanded to yield the following matrix equation

$$\lambda_i \mathbf{R} \hat{\mathbf{f}}_i = \mathbf{S} \hat{\mathbf{f}}_\mathbf{i}, \qquad [62]$$

where $\hat{\mathbf{f}}_i = \{\hat{f}_{iI}, \ldots, \hat{f}_{iN}\}^T$ is the ith eigenvector, $\boldsymbol{R} = [R_{IJ}]$, $\mathbf{S} = [S_{IJ}]$,

$$R_{IJ} = \int_{\Omega} \int_{\Omega} \Gamma(\mathbf{x}_1, \mathbf{x}_2) \Phi_I(\mathbf{x}_2) \Phi_J(\mathbf{x}_1) d\mathbf{x}_1 d\mathbf{x}_2, \quad \forall I, J = 1, \ldots, N, \qquad [63]$$

and

$$S_{IJ} = \int_{\Omega} \mathbf{\Phi}_I(\mathbf{x}) \mathbf{\Phi}_J(\mathbf{x}) d\mathbf{x}, \quad \forall I, J = 1, \ldots, N. \qquad [64]$$

Equation (62) also represents a finite dimensional analog of the integral eigenvalue problem in Eq. (47) for a multi-dimensional random field with an arbitrary domain. Equation 62 can be formulated for any covariance function and can be easily solved by standard methods of linear algebra. Hence, the meshless method is more general than the wavelet method and can solve problems involving a multi-dimensional random field with an arbitrary covariance function and an arbitrary domain. Once the eigenvector $\hat{\mathbf{f}}_i$ is calculated, Eq. (58) can be used to determine the eigenfunction $f_i(\mathbf{x})$.

Note that the meshless discretization proposed here is only intended for solving the integral eigenvalue problem, not for discretizing the random field. Matrices $\mathbf{R}$ and $\mathbf{S}$, which involve $2K$ and K dimensional integration, respectively, can be computed using standard numerical quadrature. Integration involves meshless shape functions, which are already calculated and stored for meshless stress analysis. Hence, the matrices $\mathbf{R}$ and $\mathbf{S}$ can be generated with little extra effort. However, for a large K, the computational effort in performing numerical integration can become intensive. Also note that for meshless stress analysis it is not necessary that the number and spatial distribution of nodes coincide with those for eigenfunction approximation. Different and selective discretizations can be employed, if necessary. However, in this study the same discretization was used for both meshless stress analysis and for solving the eigenvalue problem.

5. THE NEUMANN EXPANSION METHOD

5.1. Neumann Series

From Eq. (40), the discrete stochastic meshless equations are

$$\mathbf{K}(\mathbf{U})\mathbf{d}(\mathbf{U}) = \mathbf{F}, \qquad [65]$$

where $\mathbf{K}(\mathbf{U})$ and $\mathbf{d}(\mathbf{U})$ are the random stiffness matrix and the random generalized displacement vector, respectively. Using K-L expansion of $\alpha(\mathbf{x})$ from Eq. (49), it can be shown that

$$\left[\mathbf{K}^{(0)} + \sum_{i=1}^{M} U_i \mathbf{K}^{(i)} \right] \mathbf{d} = \mathbf{F}, \qquad [66]$$

where

$$\mathbf{K}^{(0)} = \prod_{l=1}^{N_c} \boldsymbol{\mathcal{M}}_{J_l}^{i_l} \left(\hat{\mathbf{k}}^{(0)} \right), \qquad [67]$$

$$\mathbf{K}^{(i)} = \prod_{l=1}^{N_c} \boldsymbol{\mathcal{M}}_{J_l}^{i_l} \left(\hat{\mathbf{k}}^{(i)} \right), \qquad [68]$$

$$\hat{\mathbf{k}}^{(0)} = \mathbf{\Lambda}^{-T} \mathbf{k}^{(0)}, \qquad [69]$$

$$\hat{\mathbf{k}}^{(i)} = \mathbf{\Lambda}^{-T} \mathbf{k}^{(i)}, \qquad [70]$$

$$\mathbf{k}^{(0)} = \begin{bmatrix} \mathbf{k}_{11}^{(0)} & \mathbf{k}_{12}^{(0)} & \cdots & \mathbf{k}_{1N}^{(0)} \\ \mathbf{k}_{21}^{(0)} & \mathbf{k}_{22}^{(0)} & \cdots & \mathbf{k}_{2N}^{(0)} \\ \vdots & \vdots & \vdots & \vdots \\ \mathbf{k}_{N1}^{(0)} & \mathbf{k}_{N2}^{(0)} & \cdots & \mathbf{k}_{NN}^{(0)} \end{bmatrix}, \quad [71]$$

and

$$\mathbf{k}^{(i)} = \begin{bmatrix} \mathbf{k}_{11}^{(i)} & \mathbf{k}_{12}^{(i)} & \cdots & \mathbf{k}_{1N}^{(i)} \\ \mathbf{k}_{21}^{(i)} & \mathbf{k}_{22}^{(i)} & \cdots & \mathbf{k}_{2N}^{(i)} \\ \vdots & \vdots & \vdots & \vdots \\ \mathbf{k}_{N1}^{(i)} & \mathbf{k}_{N2}^{(i)} & \cdots & \mathbf{k}_{NN}^{(i)} \end{bmatrix} \quad [72]$$

with

$$\mathbf{k}_{IJ}^{(0)} = \int_{\Omega} \mathbf{B}_I^T \boldsymbol{\mathcal{E}}\,[\mathbf{D}]\,\mathbf{B}_J d\Omega \quad [73]$$

and

$$\mathbf{k}_{IJ}^{(i)} = \int_{\Omega} \mathbf{B}_I^T \boldsymbol{\mathcal{E}}\,[\mathbf{D}]\,\sqrt{\lambda_i}\varphi_i(\mathbf{x})\mathbf{B}_J d\Omega. \quad [74]$$

Assume that $\mathbf{K}^{(0)}$ is positive-definite so that its inverse exists. Multiplying both sides of Eq. (66) by $[\mathbf{K}^{(0)}]^{-1}$ gives

$$\left[\mathbf{I} + \sum_{i=1}^{M} U_i \mathbf{Q}^{(i)}\right]\mathbf{d} = \mathbf{g}, \quad [75]$$

where

$$\mathbf{I} = \left[\mathbf{K}^{(0)}\right]^{-1}\mathbf{K}^{(0)}, \quad [76]$$

$$\mathbf{Q}^{(i)} = \left[\mathbf{K}^{(0)}\right]^{-1}\mathbf{K}^{(i)}, \quad [77]$$

and

$$\mathbf{g} = \left[\mathbf{K}^{(0)}\right]^{-1}\mathbf{F}. \quad [78]$$

By inverting Eq. (75),

$$\mathbf{d} = \left[\mathbf{I} + \sum_{i=1}^{M} U_i \mathbf{Q}^{(i)}\right]^{-1}\mathbf{g}. \quad [79]$$

The Neumann series expansion [25] of the right-hand side of Eq. (79) leads to

$$\mathbf{d} = \sum_{j=0}^{\infty} (-1)^j \left[\sum_{i=1}^{M} U_i \mathbf{Q}^{(i)}\right]^j \mathbf{g}, \quad [80]$$

that converges when

$$\left\| \sum_{i=1}^{M} U_i \mathbf{Q}^{(i)} \right\| < 1, \quad [81]$$

where $\|\cdot\|$ denotes some matrix norm. Theoretically, the combination of a large realization of U_i, if allowed by its probability distribution (e.g., Gaussian distribution), with λ_i may cause Eq. (81) to fail. However, for practical applications involving a small variance or an appropriately truncated distribution of $\alpha(\mathbf{x})$, Eq. (81) is usually satisfied. In that case, the mean and covariance of $\mathbf{d}$ can be calculated as follows.

5.2. Mean and Covariance of Displacement

Consider the R-order truncation of the Neumann series given by

$$\mathbf{d} = \sum_{j=0}^{R} (-1)^j \left[\sum_{i=1}^{M} U_i \mathbf{Q}^{(i)}\right]^j \mathbf{g}. \quad [82]$$

Using Eq. (82), $\mathbf{d}$ and $\mathbf{d}\mathbf{d}^T$ can be expanded as

$$\mathbf{d} = \left[\mathbf{I} - \sum_{i=1}^{M} U_i \mathbf{Q}^{(i)} + \sum_{i=1}^{M}\sum_{j=1}^{M} U_i U_j \mathbf{Q}^{(i)}\mathbf{Q}^{(j)} - \sum_{i=1}^{M}\sum_{j=1}^{M}\sum_{k=1}^{M} U_i U_j U_k \mathbf{Q}^{(i)}\mathbf{Q}^{(j)}\mathbf{Q}^{(k)} + \cdots\right]\mathbf{g} \quad [83]$$

and

$$\mathbf{d}\mathbf{d}^T = \mathbf{G} - \sum_{i=1}^{M} U_i\left\{\mathbf{Q}^{(i)}\mathbf{G} + \mathbf{G}\mathbf{Q}^{(i)T}\right\} + \sum_{i=1}^{M}\sum_{k=1}^{M} U_i U_j\left\{\mathbf{Q}^{(i)}\mathbf{Q}^{(j)}\mathbf{G} + \mathbf{Q}^{(i)}\mathbf{G}\mathbf{Q}^{(j)T} + \mathbf{G}\mathbf{Q}^{(j)T}\mathbf{Q}^{(i)T}\right\} - \cdots \quad [84]$$

where $\mathbf{G} = \mathbf{g}\mathbf{g}^T$. Let $\boldsymbol{\mu}_d = \boldsymbol{\mathcal{E}}[\mathbf{d}]$ and $\boldsymbol{\gamma}_d = \boldsymbol{\mathcal{E}}[(\mathbf{d} - \boldsymbol{\mu}_d)(\mathbf{d} - \boldsymbol{\mu}_d)^T] = \boldsymbol{\mathcal{E}}[\mathbf{d}\mathbf{d}^T] - \boldsymbol{\mu}_d\boldsymbol{\mu}_d^T$ denote the mean vector and covariance matrix, respectively, of $\mathbf{d}$. Applying the expectation operator to Eqs. (83) and (84) gives

$$\boldsymbol{\mu}_d = \left[\mathbf{I} + \sum_{i=1}^{M} \mathbf{Q}^{(i)2} + \sum_{i=1}^{M}\sum_{j=1}^{M}\left\{\mathbf{Q}^{(i)2}\mathbf{Q}^{(j)2} + \mathbf{Q}^{(i)}\mathbf{Q}^{(j)}\mathbf{Q}^{(i)}\mathbf{Q}^{(j)} + \mathbf{Q}^{(i)}\mathbf{Q}^{(j)2}\mathbf{Q}^{(i)}\right\} + \cdots\right]\mathbf{g} \quad [85]$$

and

$$\boldsymbol{\gamma}_d = \mathbf{G} + \left[\sum_{i=1}^{M}\left\{\mathbf{Q}^{(i)2}\mathbf{G} + \mathbf{Q}^{(i)}\mathbf{G}\mathbf{Q}^{(i)T} + \mathbf{G}\mathbf{Q}^{(i)T2}\right\} + \sum_{i=1}^{M}\sum_{j=1}^{M}\left\{\mathbf{Q}^{(i)2}\mathbf{Q}^{(j)2}\mathbf{G} + \mathbf{Q}^{(i)2}\mathbf{Q}^{(j)}\mathbf{G}\mathbf{Q}^{(j)T} + \mathbf{Q}^{(i)^2}\mathbf{G}\mathbf{Q}^{(j)T2}\right.\right.$$

$$+\mathbf{Q}^{(i)}\mathbf{G}\mathbf{Q}^{(j)T2}\mathbf{Q}^{(i)T}+\mathbf{G}\mathbf{Q}^{(j)T2}\mathbf{Q}^{(i)T2}+\mathbf{Q}^{(i)}\mathbf{Q}^{(j)}\mathbf{Q}^{(i)}\mathbf{Q}^{(j)}\mathbf{G}$$
$$+\mathbf{Q}^{(i)}\mathbf{Q}^{(j)}\mathbf{Q}^{(i)}\mathbf{G}\mathbf{Q}^{(j)T}+\mathbf{Q}^{(i)}\mathbf{Q}^{(j)}\mathbf{G}\mathbf{Q}^{(j)T}\mathbf{Q}^{(i)T}$$
$$+\mathbf{Q}^{(i)}\mathbf{G}\mathbf{Q}^{(j)T}\mathbf{Q}^{(i)T}\mathbf{Q}^{(j)T}+\mathbf{G}\mathbf{Q}^{(j)T}\mathbf{Q}^{(i)T}\mathbf{Q}^{(j)T}\mathbf{Q}^{(i)T}$$
$$+\mathbf{Q}^{(i)}\mathbf{Q}^{(j)2}\mathbf{Q}^{(i)}\mathbf{G}+\mathbf{Q}^{(i)}\mathbf{Q}^{(j)2}\mathbf{G}\mathbf{Q}^{(i)T}$$
$$+\mathbf{Q}^{(i)}\mathbf{Q}^{(j)}\mathbf{G}\mathbf{Q}^{(i)T}\mathbf{Q}^{(j)T}+\mathbf{Q}^{(i)}\mathbf{G}\mathbf{Q}^{(i)T}\mathbf{Q}^{(j)T2}$$
$$+\mathbf{G}\mathbf{Q}^{(i)T}\mathbf{Q}^{(j)T2}\mathbf{Q}^{(i)T}\}+\cdots\Big]-\boldsymbol{\mu}_d\boldsymbol{\mu}_d^T \qquad [86]$$

The series solutions of $\boldsymbol{\mu}_d$ and $\boldsymbol{\gamma}_d$ written above include explicit terms for $R = 4$. For larger values of R, the algebra increases significantly. The Neumann expansion method is useful when random fluctuations are small. When the coefficient of variation of $E(\mathbf{x})$ is gradually increased, $\|\sum_{i=1}^{M} U_i\mathbf{Q}^{(i)}\| \to 1$. In that case, higher-order expansions may be required for satisfactory estimates of $\boldsymbol{\mu}_d$ and $\boldsymbol{\gamma}_d$. This is one of the drawbacks of the Neumann expansion method.

Note that the generalized displacement vector d represents nodal parameters, but not the actual displacements at meshless nodes. Let $\boldsymbol{\mu}_{\hat{d}} = \mathcal{E}[\hat{\mathbf{d}}]$ and $\boldsymbol{\gamma}_{\hat{d}} = \mathcal{E}[(\hat{\mathbf{d}} - \boldsymbol{\mu}_{\hat{d}})(\hat{\mathbf{d}} - \boldsymbol{\mu}_{\hat{d}})^T]$ denote the mean vector and covariance matrix, respectively, of the nodal displacement vector $\hat{\mathbf{d}}$. From the linear relation between $\hat{\mathbf{d}}$ and $\mathbf{d}$, given by Eq. (31),

$$\boldsymbol{\mu}_{\hat{d}} = \boldsymbol{\Lambda}\boldsymbol{\mu}_d \qquad [87]$$

and

$$\boldsymbol{\gamma}_{\hat{d}} = \boldsymbol{\Lambda}\boldsymbol{\gamma}_d\boldsymbol{\Lambda}^T. \qquad [88]$$

Although similar equations can be developed for strains, for the sake of brevity they are not described here.

6. NUMERICAL EXAMPLES

Three numerical examples are presented to illustrate the proposed method. The first example involves wavelet and meshless methods for solving the integral eigenvalue problem in Eq. (47). The remaining two examples involve one- and two-dimensional stochastic-mechanics problems taken from linear elasticity. In the latter examples, K-L expansion of $\alpha(\mathbf{x})$, modeled as a homogeneous Gaussian random field, was invoked to describe the random modulus of elasticity $E(\mathbf{x})$. The wavelet or meshless method was used to calculate the eigenvalues and eigenfunctions required by K-L expansion. The Gaussian assumption implies that there is a non-zero probability of $E(\mathbf{x})$ taking on a negative value. To avoid this difficulty, the variance of the input random field was confined to a small value. Alternative representations involving truncated Gaussian distribution or other distributions suitable for a non-negative random field have been used by various researchers [26]. Such issues have not been explored in this paper, because the focus of this study was stochastic meshless analysis. A linear basis function was used for all meshless calculations. For the weight function, a value of $\beta = 2$ was selected. Both Neumann expansion and simulation methods were used to calculate second-moment characteristics of response and are described as follows.

6.1. Example 1: Eigenvalue Problem

Consider a *zero*-mean, homogeneous, one-dimensional Gaussian random field $\alpha(x)$, $0 \le x \le 1$, with covariance function $\Gamma_\alpha(\xi) = \mathcal{E}[\alpha(x)\alpha(x+\xi)]$. Three types of covariance functions,

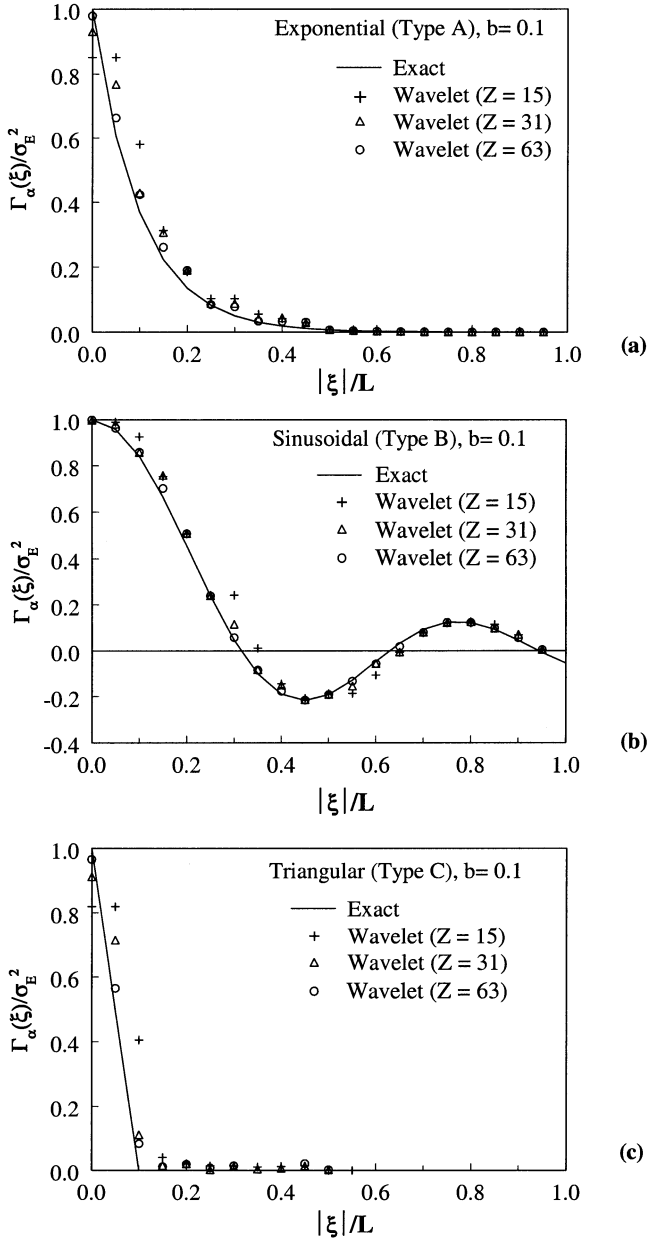

FIG. 1. Covariance functions: (a) Exponential (Type A); (b) Sinusoidal (Type B); and (c) Triangular (Type C).

defined as

$$\text{Type A:}\quad \Gamma_\alpha(\xi) = \sigma_E^2 \exp\left(-\frac{|\xi|}{bL}\right), \tag{89}$$

$$\text{Type B:}\quad \Gamma_\alpha(\xi) = \sigma_E^2 \frac{\sin\left(-\frac{|\xi|}{bL}\right)}{\frac{|\xi|}{bL}}, \tag{90}$$

and

$$\text{Type C: } \Gamma_\alpha(\xi) = \begin{cases} \sigma_E^2\left(1 - \frac{|\xi|}{bL}\right), & \frac{|\xi|}{bL} \le 1 \\ 0, & \text{otherwise} \end{cases} \tag{91}$$

were selected, where σ_E is the standard deviation of $\alpha(x)$ and b is the correlation length parameter. For numerical calculations, $\sigma_E = 0.1$ unit and $b = 0.1$ and 1.

Figure 1 shows the plots (lines) of exact normalized covariance functions for exponential (Type A), sinusoidal (Type B), and triangular models (Type C) when $b = 0.1$. Also shown are the corresponding wavelet approximations of the covariance functions using Eq. (54) for several values of expansion order $Z = 15$, 31, and 63. As expected, the wavelet approximation improves when Z increases.

Figures 2 and 3 present several eigenvalues calculated using wavelet ($Z = 15$, 31, and 63) and meshless ($N = 10$, 13, and

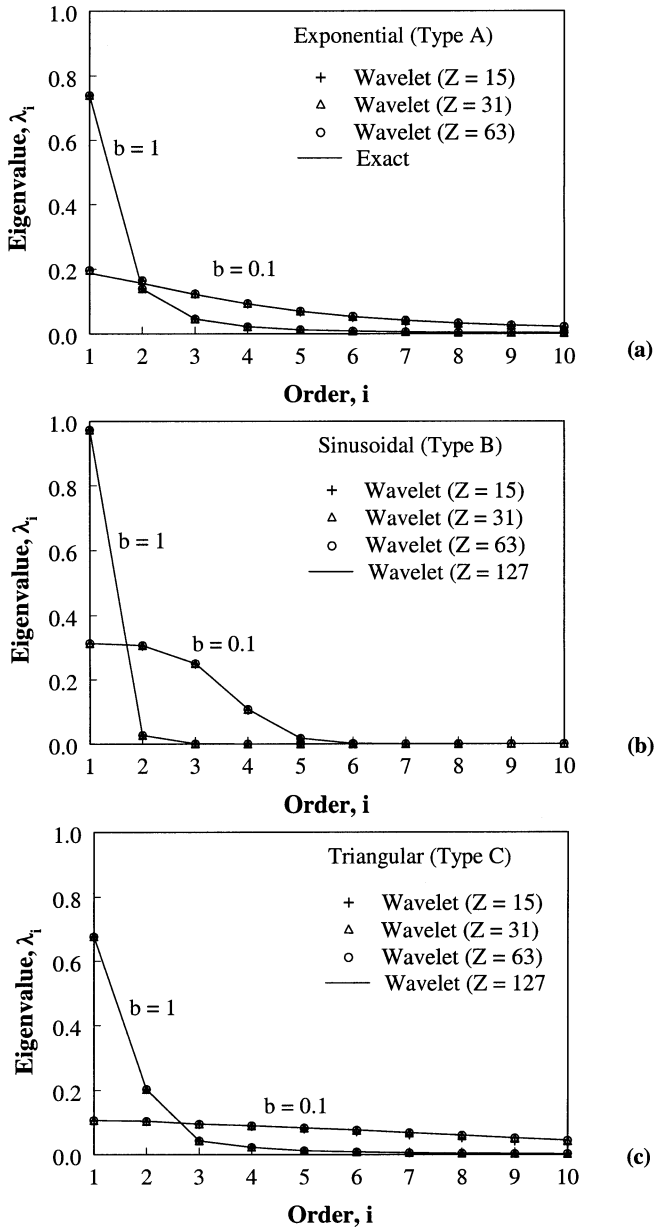

FIG. 2. Eigenvalues using wavelets: (a) Exponential (Type A); (b) Sinusoidal (Type B); and (c) Triangular (Type C).

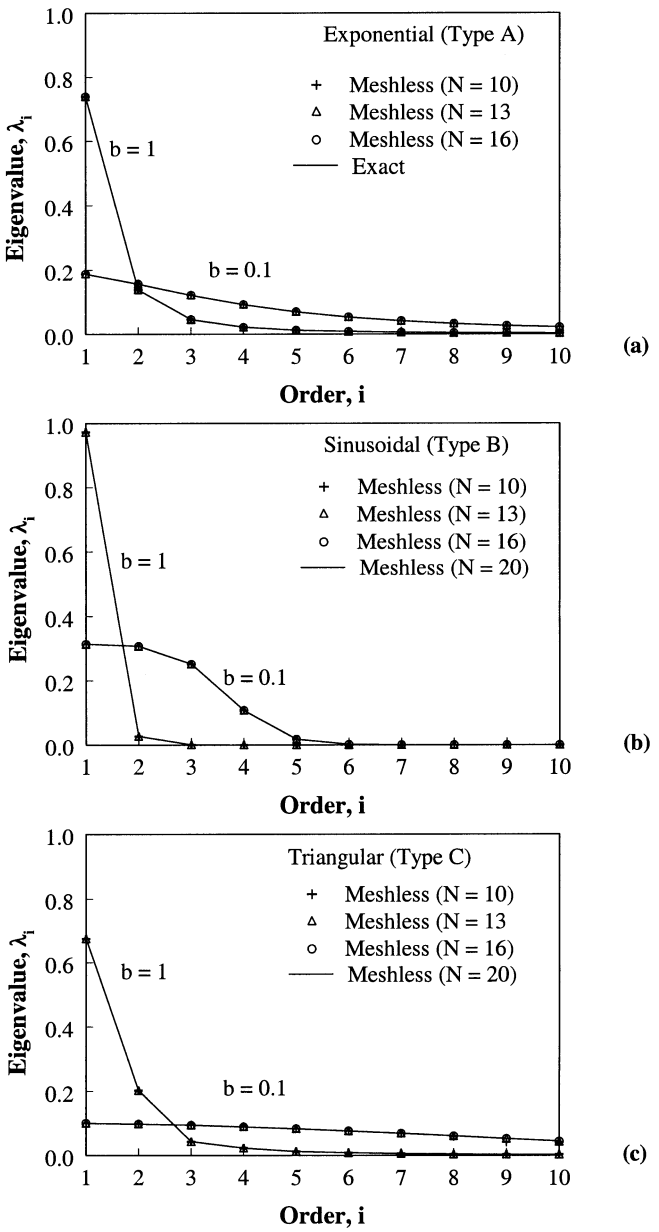

FIG. 3. Eigenvalues using meshless method: (a) Exponential (Type A); (b) Sinusoidal (Type B); and (c) Triangular (Type C).

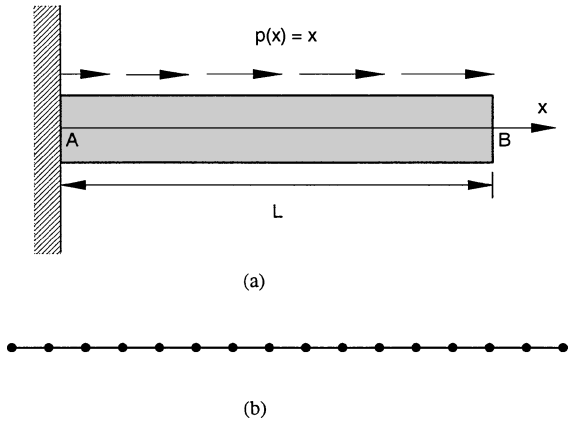

FIG. 4. A bar subjected to linear body force distribution: (a) Geometry and loads; (b) Meshless discretization (16 nodes).

16) methods for all three covariance kernels when $b = 0.1$ and 1. Clearly, the eigenvalues converge with respect to Z for the wavelet method and with respect to N for the meshless method. Also, the rate at which the magnitude of the eigenvalue decreases strongly depends on the correlation length parameter b. The smaller the value of b, the more contribution is expected from the terms associated with smaller eigenvalues. Figures 2(a) and 3(a) also present comparisons with exact eigenvalues, which are only available for the Type A covariance function [16]. For covariance functions of Types B and C, wavelet- and meshless-based eigenvalues using a large expansion order (e.g., $Z = 127$) or a large number of nodes (e.g., $N = 20$) were used to evaluate the accuracy of results associated with lower-order values of Z or N. Agreement between the eigenvalues predicted by the lower-order wavelet expansions or meshless method and the reference solution (exact solution or high-order wavelet expansion/meshless method with large N) is excellent. Similar results and observations were also made for the eigenfunctions, but are not reported here for the sake of brevity.

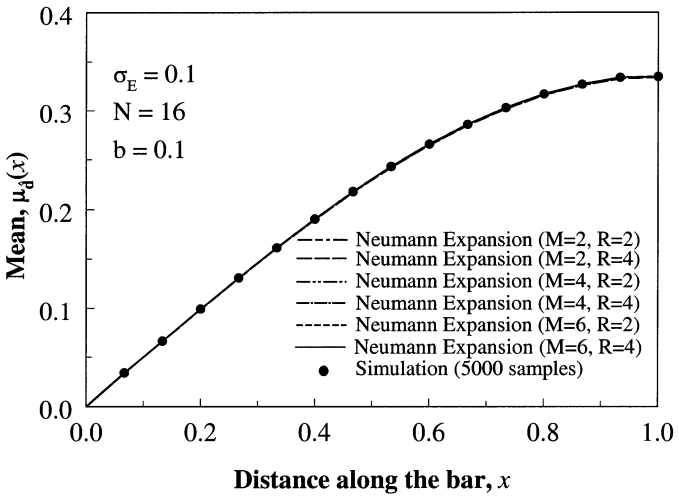

FIG. 5. Mean at distance along the bar (exponential kernel).

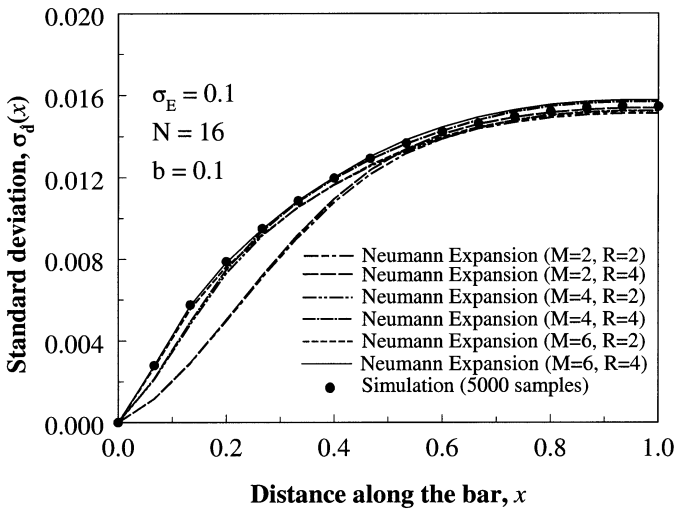

FIG. 6. Standard deviation at distance along the bar (exponential kernel).

6.2. Example 2: Response Statistics of a Bar with Linear Body Force

Consider a bar AB of length $L = 1$ unit, subjected to a linear body force distribution $p(x) = x$ in the x direction, as shown in Fig. 4(a). Point A on the bar is fixed, while point B is free. The bar has a constant cross-sectional area $A = 1$ unit. The elastic modulus $E(x) = \mu_E[1 + \alpha(x)]$ is random with mean $\mu_E = 1$ unit, and $\alpha(x)$ is a homogeneous Gaussian random field with mean zero and covariance function $\Gamma_\alpha(\xi) = \varepsilon[\alpha(x)\alpha(x + \xi)]$, where x and $x + \xi$ are the co-ordinates of two points on the bar. Three covariance functions of Types A, B, and C, defined by Eqs. (89), (90), and (91), respectively, were selected. For numerical calculations, the following values were used: $\sigma_E = 0.1$ unit and $b = 0.1$. A meshless discretization involving 16 uniformly spaced nodes is shown in Fig. 4(b).

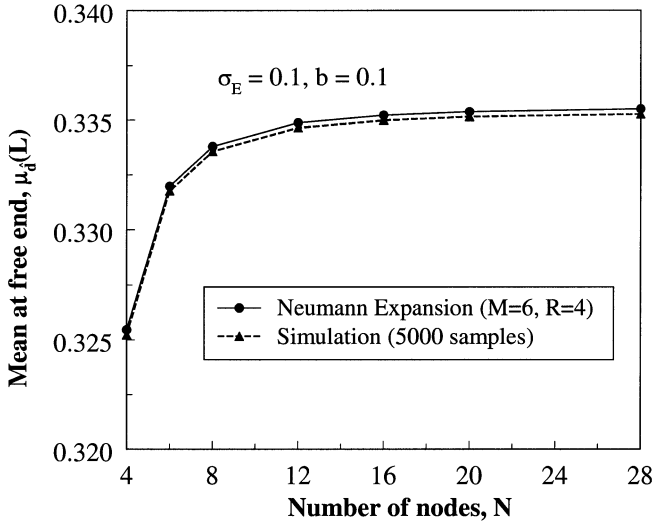

FIG. 7. Convergence of mean of displacement at free end of the bar (exponential kernel).

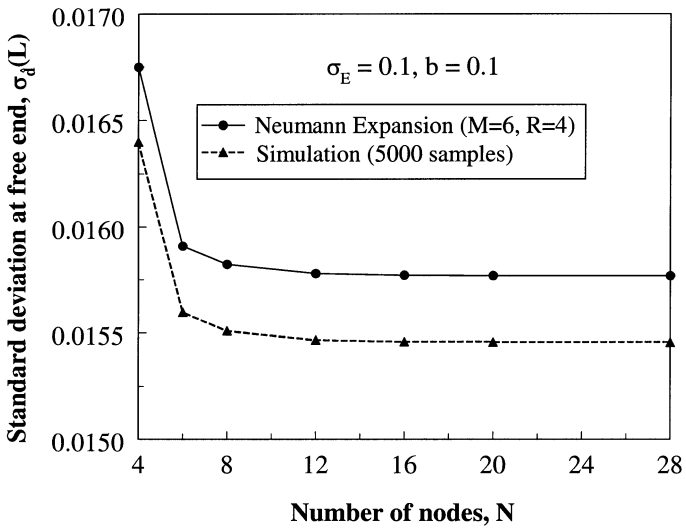

FIG. 8. Convergence of standard deviation of displacement at free end of the bar (exponential kernel).

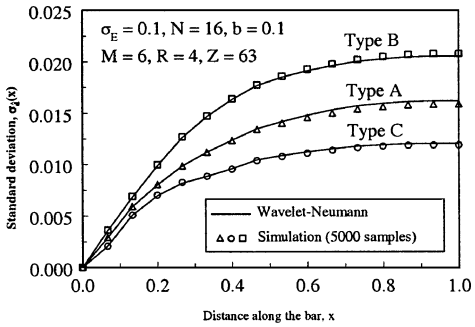

FIG. 9. Standard deviation of displacement at free end for various covariance functions.

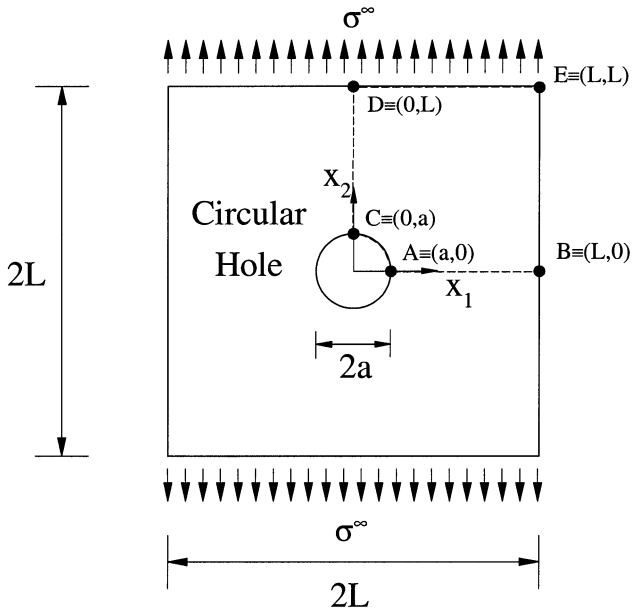

FIG. 10. A square plate with a hole subjected to uniformly distributed tension.

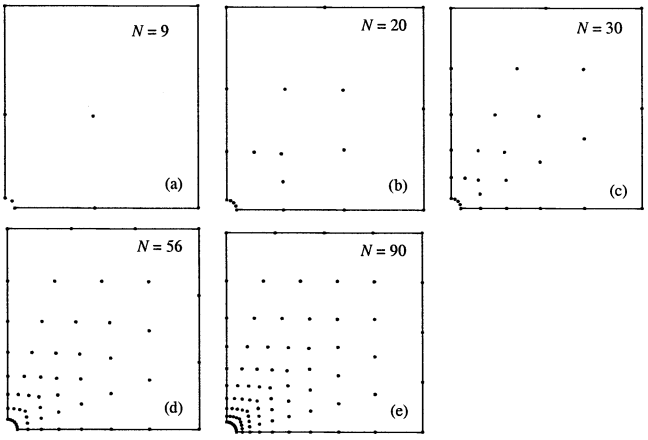

FIG. 11. Meshless discretization: (a) $N = 9$; (b) $N = 20$; (c) $N = 30$; (d) $N = 56$; (e) $N = 90$.

The stochastic meshless method developed in this study was applied to determine the first- and second-moment characteristics of the axial displacement of the bar when the covariance function of $\alpha(x)$ is Type A (exponential). For the exponential covariance function, analytical methods [16] were used to calculate the eigenvalues and eigenfunctions required in K-L expansion. Figures 5 and 6 show the mean $\mu_{\hat{d}}(x)$ and standard deviation $\sigma_{\hat{d}}(x)$, respectively, of the axial displacement as a function of x. The Neumann expansion method with various combinations of the orders of Neumann expansion (R) and K-L expansion (M) was used to predict these results. Figures 5 and 6 also show the corresponding results from the Monte Carlo simulation ($M = 6$) using 5,000 samples. When $M = 6$, K-L expansion provides accurate representation of the random field. Therefore, the above simulation results can be used as a reference solution. In Figures 5 and 6, Neumann expansion results agree very well with the simulation results. As expected, the accuracy of the Neumann expansion method improves when M and R increase.

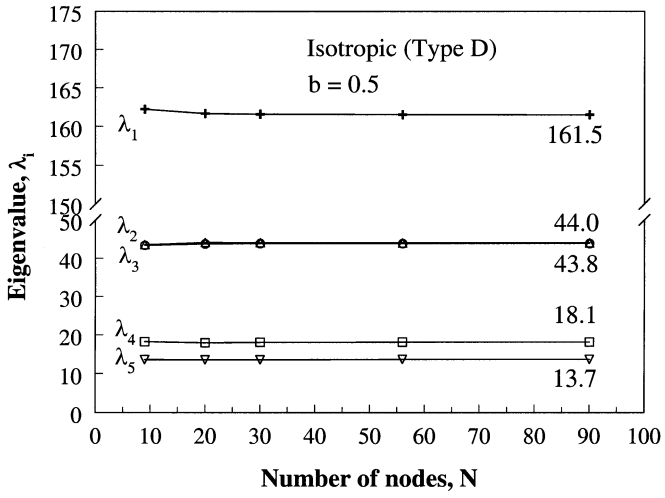

FIG. 12. Eigenvalues for isotropic covariance function (Type D) by meshless method.

To study the convergence properties of the predicted results, additional stochastic meshless analyses were performed by increasing the number of nodes (N) from 4 to 28. For each value of N, a uniform spacing was used for meshless discretization of the bar. The same inputs defined earlier were also used for each analysis. Figures 7 and 8 show the predicted mean $[\mu_{\hat{d}}(L)]$ and standard deviation $[\sigma_{\hat{d}}(L)]$ of the axial displacement at the free end (point B) as a function of N. The results of Neumann expansion using $M = 6$, $R = 4$ and of the simulation method using $M = 6$ and 5,000 samples are shown. Indeed, the stochastic meshless method yields convergent solutions of mean and standard deviation of the response.

Figure 9 shows the standard deviation of the displacement as a function of x for all three covariance functions using wavelet and K-L expansions. The Neumann expansion method with $R = 4$, $M = 6$, and $Z = 63$ was used to generate the line plots in Fig. 9. Again, the selected orders of expansions and approximations are large enough to produce a convergent solution of the response. Figure 9 also shows the corresponding results from Monte Carlo simulation ($M = 6$, $Z = 63$) using 5,000 samples. The Neumann expansion results agree very well with the simulation results.

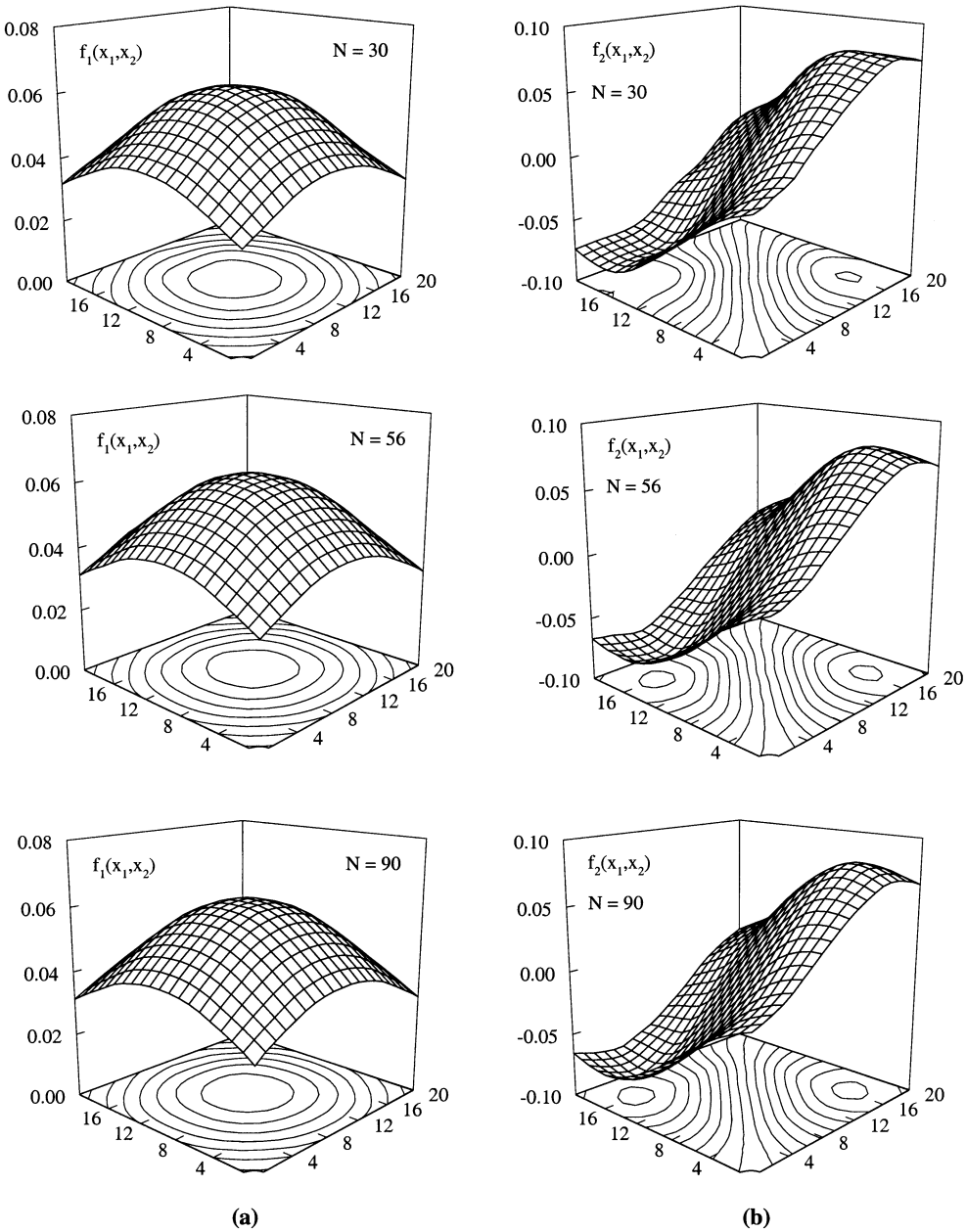

FIG. 13. First and second eigenfunctions for isotropic covariance kernel (Type D) by meshless method; (a) $f_1(\mathbf{x})$; (b) $f_2(\mathbf{x})$.

6.3. Example 3: Response Statistics of a Square Plate with a Circular Hole Under Tension

Consider a square plate with a circular hole, as shown in Figure 10. The plate has dimension $2L = 40$ units, a hole with diameter $2a = 2$ units, and is subjected to a uniformly distributed load of magnitude $\sigma^{\infty} = 1$ unit. The Poisson's ratio ν was chosen as 0.3. The elastic modulus was assumed to be a random field and symmetrically distributed with respect to x_1- and x_2-axes (see Fig. 10). The modulus of elasticity $E(\mathbf{x})$ was represented by $E(\mathbf{x}) = \mu_E[1 + \alpha(\mathbf{x})]$, where $\mu_E = 1$ unit is the constant mean over the domain Ω and $\alpha(\mathbf{x})$ is a homogeneous Gaussian random field with mean *zero* and covariance function $\Gamma_\alpha(\xi) = \mathcal{E}[\alpha(\mathbf{x})\alpha(\mathbf{x}+\boldsymbol{\xi})]$, where $\mathbf{x} \equiv (x_1, x_2)$ and $\mathbf{x} + \boldsymbol{\xi} \equiv (x_1 + \xi_1, x_2 + \xi_2)$ are the co-ordinates of two points in the domain Ω of the quarter plate represented by region ABEDC and shaded in Fig. 10. Due to symmetry, only a quarter of the plate needs to be analyzed. Figures 11(a)–11(e) show five meshless discretizations of the quarter plate with the total number of nodes $N = 9$, 20, 30, 56, and 90, which represent progressively increasing degrees of meshless refinement.

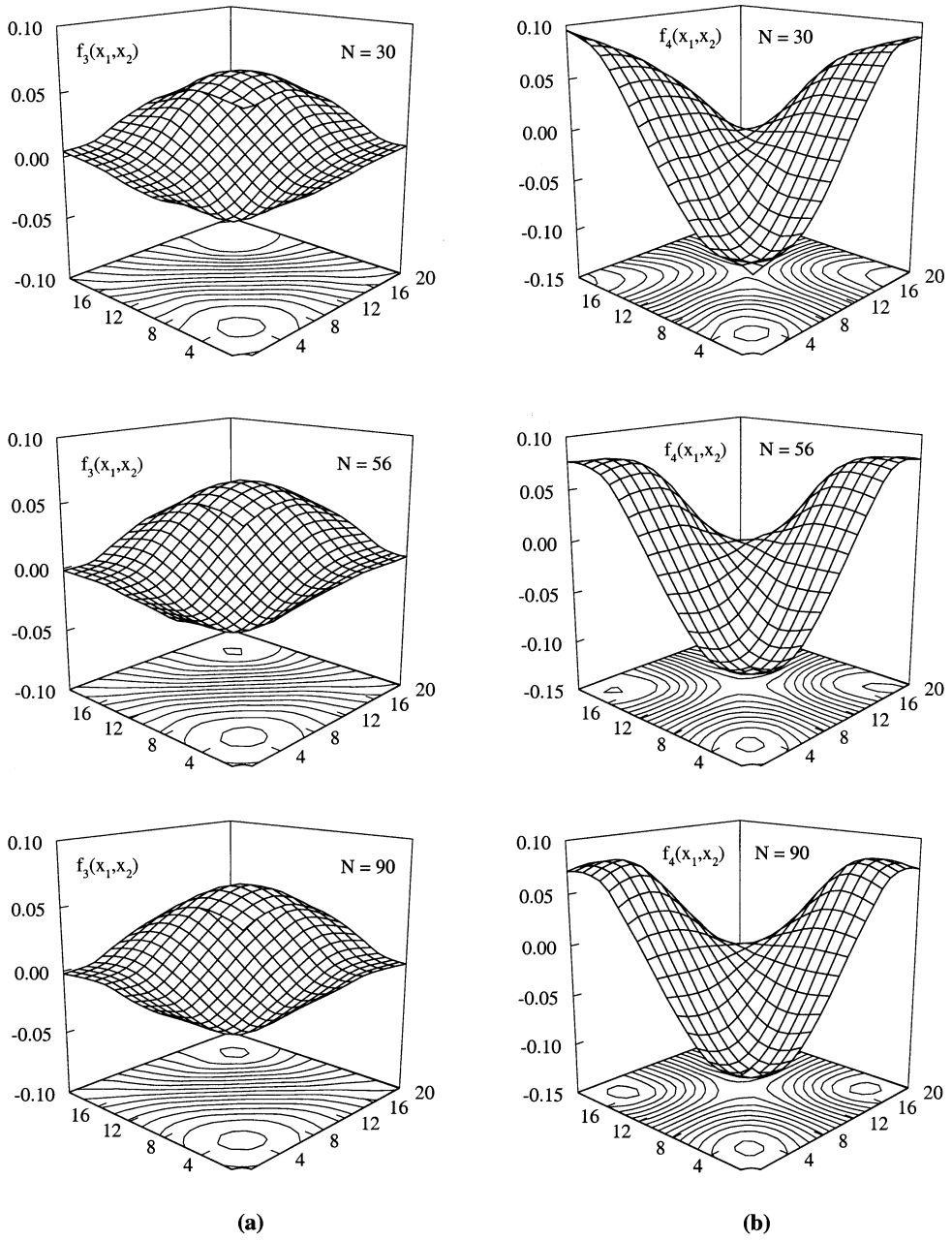

FIG. 14. Third and fourth eigenfunctions for isotropic covariance kernel (Type D) by meshless method; (a) $f_3(\mathbf{x})$; (b) $f_4(\mathbf{x})$.

For the quarter plate ABEDC, four types of covariance functions of $\alpha(\mathbf{x})$, defined by

Type A:

$$\Gamma_\alpha(\xi) = \sigma_E^2 \exp\left(-\frac{|\xi_1|}{b_1 L} - \frac{|\xi_2|}{b_2 L}\right), \quad \forall \mathbf{x}, \quad \mathbf{x}+\boldsymbol{\xi} \in \Omega \qquad [92]$$

Type B:

$$\Gamma_\alpha(\xi) = \sigma_E^2 \frac{\sin\left(\frac{|\xi_1|}{b_1 L}\right)\sin\left(\frac{|\xi_2|}{b_2 L}\right)}{\frac{|\xi_1|}{b_1 L}\frac{|\xi_2|}{b_2 L}}, \quad \forall \mathbf{x}, \quad \mathbf{x}+\boldsymbol{\xi} \in \Omega, \qquad [93]$$

Type C:

$$\Gamma_\alpha(\boldsymbol{\xi}) = \sigma_E^2 \left(1 - \frac{|\xi_1|}{b_1 L}\right)\left(1 - \frac{|\xi_2|}{b_2 L}\right), \quad \forall \mathbf{x}, \quad \mathbf{x}+\boldsymbol{\xi} \in \Omega \qquad [94]$$

and

$$\text{Type D: } \Gamma_\alpha(\boldsymbol{\xi}) = \sigma_E^2 \exp\left(-\frac{\|\boldsymbol{\xi}\|}{bL}\right), \quad \forall \mathbf{x}, \quad \mathbf{x}+\boldsymbol{\xi} \in \Omega, \qquad [95]$$

were selected, where $\sigma_E = 0.1$ unit and $b = b_1 = b_2 = 0.5$. Of these four covariance kernels, the first three are separable (i.e., they satisfy Eq. (57)), but the last is an inseparable kernel and belongs to the class of isotropic random fields. However, in all four cases, the domain of the random field is not rectangular. Hence, the wavelet-based method using one-dimensional EHW basis functions cannot be used to solve the eigenvalue problem. Consequently, the meshless method developed here is needed and was used for the following calculations.

Figure 12 shows several eigenvalues calculated using the meshless method (Eqs. (58–64)) for $N = 9$, 20, 30, 56, and 90, for the Type D covariance kernel. Clearly, the eigenvalues converge with respect to N, as expected. Similar comparisons of the first four eigenfunctions $f_1(\mathbf{x})$, $f_2(\mathbf{x})$, $f_3(\mathbf{x})$, and $f_4(\mathbf{x})$, presented in Figs. 13(a), 13(b), 14(a), and 14(b), respectively, also demonstrate the convergence of eigenfunctions with respect to N. These convergent solutions of eigenvalues and eigenfunctions provide confidence in the following probabilistic results when $N = 90$. Note that there is no analytical eigensolution available for the Type D covariance function with an arbitrary, non-rectangular domain.

Using the finest discretization with $N = 90$ [Fig. 11(e)] considered here, Tables 1, 2, 3, and 4 present the mean and standard deviation of various displacements and/or strains at points A, B, C, D, and E (see Fig. 10), when $\alpha(\mathbf{x})$ has Types A, B, C, and D covariance functions, respectively. Both Neumann expansion and simulation methods were employed to calculate these statistics. For both methods, meshless discretization was used to calculate the eigenvalues and eigenfunctions required for K-L expansion. The order of K-L expansion in both methods was chosen to be $M = 12$ and was verified to be large enough to represent the random field adequately. For the Neumann expansion method, the value of $R = 4$ was used. For the simulation method, the sample size was 5,000. According to Tables 1–4, the response

TABLE 1
Mean and standard deviation of displacements and/or strains for exponential covariance function (Type A, $\sigma_E = 0.1$, $b_1 = b_2 = 0.5$)

		Neumann expansion ($M = 12$, $R = 4$)		Monte Carlo simulation ($M = 12$, 5000 Samples)	
Location	Response[a]	Mean	Standard deviation	Mean	Standard deviation
A	u_1	-9.75×10^{-1}	1.12×10^{-1}	-9.76×10^{-1}	1.12×10^{-1}
	ε_{11}	-3.21×10^{-1}	2.60×10^{-2}	-3.21×10^{-1}	2.56×10^{-2}
	ε_{22}	2.95	2.40×10^{-1}	2.95	2.37×10^{-1}
	ε_{12}	-3.96×10^{-1}	3.29×10^{-2}	-3.96×10^{-1}	3.25×10^{-2}
B	u_1	-6.20	4.65×10^{-1}	-6.20	4.61×10^{-1}
	ε_{22}	9.97×10^{-1}	8.00×10^{-2}	9.99×10^{-1}	8.21×10^{-2}
C	u_2	2.97	2.50×10^{-1}	2.97	2.46×10^{-1}
	ε_{11}	-7.17×10^{-1}	8.68×10^{-2}	-7.18×10^{-1}	8.72×10^{-2}
	ε_{22}	1.39×10^{-1}	1.29×10^{-2}	1.39×10^{-1}	1.28×10^{-2}
	ε_{12}	3.53×10^{-1}	3.91×10^{-2}	3.53×10^{-1}	3.90×10^{-2}
D	u_2	2.04×10^{1}	1.34	2.04×10^{1}	1.33
	ε_{22}	9.89×10^{-1}	8.32×10^{-2}	9.88×10^{-1}	8.34×10^{-2}
E	u_1	-5.84	5.97×10^{-1}	-5.84	5.99×10^{-1}
	u_2	1.99×10^{1}	1.38	1.99×10^{1}	1.38
	ε_{22}	9.78×10^{-1}	8.40×10^{-2}	9.78×10^{-1}	8.37×10^{-2}

[a] u_1 and u_2 represent horizontal and vertical displacements, respectively. ε_{11} and ε_{22} represent normal strains in x_1 and x_2 directions, respectively; and ε_{12} represents shear strain.

TABLE 2
Mean and standard deviation of displacements and/or strains for sinusoidal covariance function (Type B, $\sigma_E = 0.1$, $b_1 = b_2 = 0.5$)

		Neumann expansion ($M = 12$, $R = 4$)		Monte Carlo simulation ($M = 12$, 5000 Samples)	
Location	Response[a]	Mean	Standard deviation	Mean	Standard deviation
A	u_1	-9.78×10^{-1}	1.16×10^{-1}	-9.78×10^{-1}	1.16×10^{-1}
	ε_{11}	-3.22×10^{-1}	3.34×10^{-2}	-3.22×10^{-1}	3.29×10^{-2}
	ε_{22}	2.96	3.06×10^{-1}	2.96	3.02×10^{-1}
	ε_{12}	-3.97×10^{-1}	4.13×10^{-2}	-3.97×10^{-1}	4.09×10^{-2}
B	u_1	-6.22	6.25×10^{-1}	-6.22	6.19×10^{-1}
	ε_{22}	1.00	9.84×10^{-2}	1.00	9.74×10^{-2}
C	u_2	2.98	3.08×10^{-1}	2.98	3.05×10^{-1}
	ε_{11}	-7.20×10^{-1}	8.98×10^{-2}	-7.21×10^{-1}	9.00×10^{-2}
	ε_{22}	1.39×10^{-1}	1.57×10^{-2}	1.40×10^{-1}	1.57×10^{-2}
	ε_{12}	3.54×10^{-1}	4.09×10^{-2}	3.54×10^{-1}	4.09×10^{-2}
D	u_2	2.04×10^{1}	1.96	2.04×10^{1}	1.96
	ε_{22}	9.92×10^{-1}	9.86×10^{-2}	9.93×10^{-1}	9.91×10^{-2}
E	u_1	-5.86	6.81×10^{-1}	-5.87	6.85×10^{-1}
	u_2	2.00×10^{1}	1.94	2.00×10^{1}	1.95
	ε_{22}	9.81×10^{-1}	1.01×10^{-1}	9.82×10^{-1}	1.02×10^{-1}

[a] u_1 and u_2 represent horizontal and vertical displacements, respectively. ε_{11} and ε_{22} represent normal strains in x_1 and x_2 directions, respectively; and ε_{12} represents shear strain.

TABLE 3
Mean and standard deviation of displacements and/or strains for triangular covariance function (Type C, $\sigma_E = 0.1$, $b_1 = b_2 = 0.5$)

		Neumann expansion ($M = 12$, $R = 4$)		Monte Carlo simulation ($M = 12$, 5000 Samples)	
Location	Response[a]	Mean	Standard deviation	Mean	Standard deviation
A	u_1	-9.75×10^{-1}	1.24×10^{-1}	-9.75×10^{-1}	1.23×10^{-1}
	ε_{11}	-3.21×10^{-1}	2.65×10^{-2}	-3.21×10^{-1}	2.61×10^{-2}
	ε_{22}	2.95	2.41×10^{-1}	2.95	2.38×10^{-1}
	ε_{12}	-3.96×10^{-1}	3.31×10^{-2}	-3.96×10^{-1}	3.27×10^{-2}
B	u_1	-6.20	4.19×10^{-1}	-6.19	4.08×10^{-1}
	ε_{22}	9.97×10^{-1}	8.23×10^{-2}	9.98×10^{-1}	8.19×10^{-2}
C	u_2	2.97	2.49×10^{-1}	2.97	2.46×10^{-1}
	ε_{11}	-7.17×10^{-1}	9.64×10^{-2}	-7.18×10^{-1}	9.59×10^{-2}
	ε_{22}	1.39×10^{-1}	1.34×10^{-2}	1.39×10^{-1}	1.34×10^{-2}
	ε_{12}	3.53×10^{-1}	4.20×10^{-2}	3.53×10^{-1}	4.16×10^{-2}
D	u_2	2.03×10^{1}	1.09	2.03×10^{1}	1.06
	ε_{22}	9.89×10^{-1}	8.30×10^{-2}	9.88×10^{-1}	8.13×10^{-2}
E	u_1	-5.84	5.66×10^{-1}	-5.85	5.65×10^{-1}
	u_2	1.99×10^{1}	1.16	1.99×10^{1}	1.16
	ε_{22}	9.78×10^{-1}	8.12×10^{-2}	9.78×10^{-1}	8.25×10^{-2}

[a] u_1 and u_2 represent horizontal and vertical displacements, respectively. ε_{11} and ε_{22} represent normal strains in x_1 and x_2 directions, respectively; and ε_{12} represents shear strain.

TABLE 4
Mean and standard deviation of displacements and/or strains for isotropic covariance function (Type D, $\sigma_E = 0.1$, $b = 0.5$)

		Neumann expansion ($M = 12$, $R = 4$)		Monte Carlo simulation ($M = 12$, 5000 Samples)	
Location	Response[a]	Mean	Standard deviation	Mean	Standard deviation
A	u_1	-9.76×10^{-1}	1.18×10^{-1}	-9.77×10^{-1}	1.19×10^{-1}
	ε_{11}	-3.21×10^{-1}	2.79×10^{-2}	-3.22×10^{-1}	2.79×10^{-2}
	ε_{22}	2.95	2.58×10^{-1}	2.95	2.58×10^{-1}
	ε_{12}	-3.96×10^{-1}	3.53×10^{-2}	-3.97×10^{-1}	3.54×10^{-2}
B	u_1	-6.20	4.97×10^{-1}	-6.21	4.95×10^{-1}
	ε_{22}	9.98×10^{-1}	8.62×10^{-2}	9.99×10^{-1}	8.49×10^{-2}
C	u_2	2.97	2.66×10^{-1}	2.97	2.66×10^{-1}
	ε_{11}	-7.18×10^{-1}	9.16×10^{-2}	-7.19×10^{-1}	9.28×10^{-2}
	ε_{22}	1.39×10^{-1}	1.39×10^{-2}	1.39×10^{-1}	1.41×10^{-2}
	ε_{12}	3.53×10^{-1}	4.09×10^{-2}	3.54×10^{-1}	4.13×10^{-2}
D	u_2	2.04×10^{1}	1.45	2.04×10^{1}	1.44
	ε_{22}	9.90×10^{-1}	8.78×10^{-2}	9.88×10^{-1}	8.52×10^{-2}
E	u_1	-5.85	6.07×10^{-1}	-5.84	5.98×10^{-1}
	u_2	1.99×10^{1}	1.48	1.99×10^{1}	1.46
	ε_{22}	9.79×10^{-1}	8.79×10^{-2}	9.78×10^{-1}	8.59×10^{-2}

[a] u_1 and u_2 represent horizontal and vertical displacements, respectively. ε_{11} and ε_{22} represent normal strains in x_1 and x_2 directions, respectively; and ε_{12} represents shear strain.

statistics from the Neumann expansion method match very well with the simulation results. For $M > 12$, changes in the statistics by both methods were so small that the statistics in Table 1–4 can be viewed as convergent results. The details of the convergence study are not reported here for the sake of brevity.

CONCLUSIONS

This paper presents a stochastic meshless method for probabilistic analysis of linear-elastic structures with spatially varying random material properties. Using Karhunen-Loève expansion, the homogeneous random field representing material properties was discretized by a set of orthonormal eigenfunctions and uncorrelated random variables. Two numerical methods were developed for solving the integral eigenvalue problem associated with Karhunen-Loève expansion. In the first method, the eigenfunctions were approximated as linear sums of wavelets and the integral eigenvalue problem was converted to a finite-dimensional matrix eigenvalue problem that can be easily solved. This method facilitates the calculation of eigenfunctions for any covariance kernel of a one-dimensional random field, but only for a separable covariance kernel of a multi-dimensional random field. Consequently, a second method was developed for a multi-dimensional random field with any arbitrary covariance function. By using a Galerkin approach in conjunction with meshless discretization, the integral eigenvalue problem was also converted to a matrix eigenvalue problem. The second method is more general than the first and can solve problems involving a multi-dimensional random field with arbitrary covariance functions. In conjunction with meshless discretization, the classical Neumann expansion method was applied to predict second-moment characteristics of the structural response. Several numerical examples are presented to examine the accuracy and convergence of the stochastic meshless method. A good agreement is obtained between the results of the proposed method and the Monte Carlo simulation. Since mesh generation of complex structures can be far more time-consuming and costly than the solution of a discrete set of equations, the meshless method provides an attractive alternative to the finite element method for solving stochastic-mechanics problems.

REFERENCES

1. Monaghan, J. J., "An introduction to SPH," *Computer Physics Communications* **48**, 89–96 (1988).
2. Liew, K. M., Huang, Y. Q., and Reddy, J. N., "A hybrid moving least squares and differential quadrature (MLSDQ) meshfree method," *International Journal of Computational Engineering Science* **3**(1), 1–12 (2002).
3. Nayroles, B., Touzot, G., and Villon, P., "Generalizing the finite element method: Diffuse approximation and diffuse elements," *Computational Mechanics* **10**, 307–318 (1992).
4. Belytschko, T., Lu, Y. Y., and Gu, L., "Element-free galerkin methods," *International Journal for Numerical Methods in Engineering* **37**, 229–256 (1994).
5. Duarte, C. A. M., and Oden, J. T., "H-p clouds—an h-p meshless method," *Numerical Methods for Partial Differential Equations* **12**(6), 673–705 (1996).
6. Melenk, J. M., and Babuska, I., "The partition of unity finite element method: Basic theory and applications," *Computer Methods in Applied Mechanics and Engineering* **139**, 280–314 (1996).

7. Liu, W. K., Jun, S., and Zhang, Y. F., "Reproducing kernel particle methods," *International Journal for Numerical Methods in Fluids* **20**, 1081–1106 (1995).
8. Atluri, S. N., and Zhu, T., "A new meshless local petrov-galerkin (MLPG) Approach," *Computational Mechanics* **22**, 117–127 (1998).
9. Lancaster, P., and Salkauskas, K., "Surfaces generated by moving least squares methods," *Mathematics of Computation* **37**, 141–158 (1981).
10. Belytschko, T., Lu, Y. Y., and Gu, L., "Crack propagation by element-free galerkin methods," *Engineering Fracture Mechanics* **51**(2), 295–315 (1995).
11. Rao, B. N., and Rahman, S., "An efficient meshless method for fracture analysis of cracks," *Computational Mechanics* **26**, 398–408 (2000).
12. Rahman, S., and Rao, B. N., "A perturbation method for stochastic meshless analysis in elastostatics," *International Journal for Numerical Methods in Engineering* **50**(8), 1969–1991 (2001).
13. Rahman, S., and Rao, B. N., "An element-free galerkin method for probabilistic mechanics and reliability," *International Journal of Solids and Structures* **38**, 9313–9330 (2001).
14. Chen, J. S., and Wang, H. P., "New boundary condition treatments for meshless computation of contact problems," *Computer Methods in Applied Mechanics and Engineering* **187**, 441–468 (2000).
15. Lu, Y. Y., Belytschko, T., and Gu, L., "A new implementation of the element free galerkin method," *Computer Methods in Applied Mechanics and Engineering* **113**, 397–414 (1994).
16. Ghanem, P. D., and Spanos, P. D., *Stochastic Finite Element: A Spectral Approach*, Springer-Verlag, New York (1991).
17. Lawrence, M. A., "Basis random variables in finite element analysis," *International Journal for Numerical Methods in Engineering* **24**, 1849–1863 (1987).
18. Der Kiureghian, A., and Liu, P.-L., "Structural reliability under incomplete probability information," *ASCE Journal of Engineering Mechanics* **112**(1), 85–104 (1986).
19. Vanmarcke, E. H., and Grigoriu, M., "Stochastic finite element analysis of simple beams," *ASCE Journal of Engineering Mechanics* **109**(5), 1203–1214 (1983).
20. Liu, W. K., Belytschko, T., and Mani, A., "Random Fields Finite Element," *International Journal for Numerical Methods in Engineering* **23**, 1831–1845 (1986).
21. Deodatis, G., "Weighted integral method I: Stochastic stiffness matrix," *ASCE Journal of Engineering Mechanics* **117**(8), 1851–1864 (1991).
22. Li, C.-C., and Der Kiureghian, A., "Optimal discretization of random fields," *ASCE Journal of Engineering Mechanics* **119**(6), 1136–1154 (1992).
23. Davenport, W. B., and Root, W. L., *An Introduction to the Theory of Random Signals and Noise*, McGraw-Hill, New York (1958).
24. Mei, H., and Agrawal, O. P., "Wavelet-based model for stochastic analysis of beam structures," *AIAA Journal* **36**(3), 465–470 (1998).
25. Adomian, G., and Malakian, K., "Inversion of stochastic partial differential operators—the linear case," *Journal of Mathematical Analysis and Applications* **77**(2), 505–512 (1980).
26. IASSAR Subcommittee on Computational stochastic Structural Mechanics, "A state-of-the-art report on computational stochastic mechanics," *Probabilistic Engineering Mechanics*, edited by G. I. Schueller **12**(4), 197–321 (1997).